



Thin-film flow due to an asymmetric distribution of surface tension and applications to surfactant deposition

Jun Eshima¹, Luc Deike^{1,2,†} and Howard A. Stone^{1,†}

¹Department of Mechanical and Aerospace Engineering, Princeton University, Princeton, NJ 08544, USA

²High Meadows Environmental Institute, Princeton University, Princeton, NJ 08544, USA

(Received 31 October 2023; revised 13 May 2024; accepted 16 May 2024)

Thin-film equations are utilised in many different areas of fluid dynamics when there exists a direction in which the aspect ratio can be considered small. We consider thin free films with Marangoni effects in the extensional flow regime, where velocity gradients occur predominantly along the film. In practice, because of the local deposition of surfactants or input of energy, asymmetric distributions of surfactants or surface tension more generally, are possible. Such examples include the surface of bubbles and the rupture of thin films. In this study, we consider the asymmetric thin-film equations for extensional flow with Marangoni effects. Concentrating on the case of small Reynolds number Re , we study the deposition of insoluble surfactants on one side of a liquid sheet otherwise at rest and the resulting thinning and rupture of the sheet. The analogous problem with a uniformly thinning liquid sheet is also considered. In addition, the centreline deformation is discussed. In particular, we show analytically that if the surface tension isotherm $\sigma = \sigma(\Gamma)$ is nonlinear (surface tension σ varies with surfactant concentration Γ), then accounting for top–bottom asymmetry leads to slower (faster) thinning and pinching if $\sigma = \sigma(\Gamma)$ is convex (concave). The analytical progress reported in this paper allows us to discuss the production of satellite drops from rupture via Marangoni effects, which, if relevant to surface bubbles, would be an aerosol production mechanism that is distinct from jet drops and film drops.

Key words: thin films, capillary flows

† Email addresses for correspondence: hastone@princeton.edu, ldeike@princeton.edu

© The Author(s), 2024. Published by Cambridge University Press. This is an Open Access article, distributed under the terms of the Creative Commons Attribution licence (<http://creativecommons.org/licenses/by/4.0>), which permits unrestricted re-use, distribution and reproduction, provided the original article is properly cited.

1. Introduction

1.1. Background

Thin-film equations are utilised in fluid dynamics when there exists a direction in which the aspect ratio can be considered small (Oron, Davis & Bankoff 1997; Craster & Matar 2009; Eggers & Fontelos 2015). Examples include bubble caps, tear films, ice sheets and lubrication configurations. In particular, thin-film equations have been used to consider flows influenced by surface tension variations (De Wit, Gallez & Christov 1994; Breward 1999; Timmermans & Lister 2002; Bowen & Tilley 2013; Kitavtsev, Fontelos & Eggers 2018). Such Marangoni flows are responsible for many different physical processes across varied lengthscales, such as the calming of surface ocean waves, tears of wine, and the decrease in velocity of a rising bubble (Manikantan & Squires 2020).

Recently, Marangoni effects have been suggested as a potential mechanism for rupture of surface bubbles (Poulain, Villermaux & Bourouiba 2018), which refers to bubbles that rest near a liquid–vapour interface. The caps of such surface bubbles are thin liquid films. It has been noted theoretically (Bowen & Tilley 2013; Kitavtsev *et al.* 2018) and experimentally (Néel & Villermaux 2018) that a sufficiently large local deposition of surfactants or (heat) onto a liquid film is enough to rupture the film. Surface bubble rupture is of importance in industry, health (Bourouiba 2021), volcanic activity (Gonnermann & Manga 2007; Nguyen *et al.* 2013) and ocean–atmosphere interaction (Veron 2015; Deike 2022). Once emitted in the atmosphere, aerosols formed from the rupture of ocean surface bubbles can serve as cloud condensate nuclei and affect the radiative balance of Earth.

In studies of thin films influenced by Marangoni effects, top–bottom symmetry is often assumed (De Wit *et al.* 1994; Bowen & Tilley 2013; Kitavtsev *et al.* 2018). In practice, asymmetric, i.e. top to bottom in the case of a horizontal sheet and side to side in the case of a vertical sheet, distributions of surfactants, or surface tension more generally, are possible. An immediate consequence of assuming symmetry is that the bending of the sheet, i.e. the centreline deformation, is ignored. For a nonlinear surface tension isotherm $\sigma = \sigma(\Gamma)$, indicating how surface tension σ varies with surfactant concentration Γ , we expect that $\sigma(\Gamma) \neq 2\sigma(\frac{1}{2}\Gamma)$ in general. Thus, modelling an asymmetric set-up, e.g. surfactant concentration Γ on the top surface and zero surfactant concentration on the bottom surface, with a symmetric configuration, where the surfactant concentration is $\frac{1}{2}\Gamma$ on both the top and bottom surfaces, may potentially lead to inaccurate tangential Marangoni forces, which will be discussed in § 4.6 below.

We consider the extensional flow regime, where the velocity (and pressure) in the direction of the large length scale can be taken to be roughly independent of the small direction. This flow regime is amenable to theoretical analysis but places restrictions (see § 3.2) on the magnitude of the Reynolds number (comparing inertia and viscous forces), Marangoni number (comparing Marangoni and viscous forces) and capillary number (comparing viscous and capillary forces).

The broken symmetry in surface tension means that the bending of the sheet should be considered. Centreline deformation of thin films has been discussed in the literature. For example, a heavy liquid filament sags under the influence of gravity (Teichman & Mahadevan 2003). Folding liquid sheets are also an example (Ribe 2002, 2003). A well known phenomenon for thin liquid sheets with top–bottom asymmetry is the flapping of a retracting liquid sheet (Lhuissier & Villermaux 2009), which has been proposed recently to be relevant for the production of film drops (Jiang *et al.* 2022).

In the context of surface bubbles, the inside of a bubble and the outside of a bubble can have different distributions of surfactants. Indeed, top–bottom asymmetry of a surface bubble with surfactants can be seen in numerical work by Atasi *et al.* (2020) and in

Asymmetric Marangoni flow

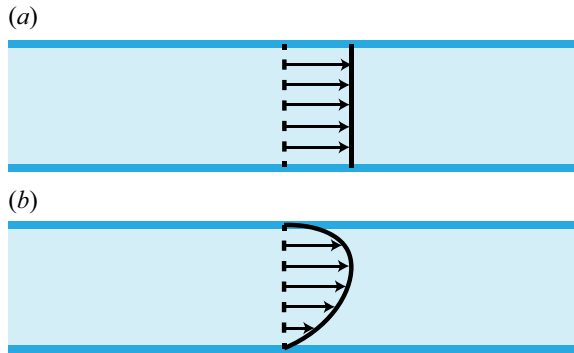


Figure 1. Schematic diagram of the (a) extensional flow regime and (b) shear flow regime (non-extensional flow).

experimental work by Zawala *et al.* (2023). Theoretically, Shi, Fuller & Shaqfeh (2022) considered the drainage of a surface bubble with surfactants, where their derivation also considered extensional flow with top–bottom asymmetry (without inertia, similar to Breward 1999). In their subsequent analysis and experimental verification of their extensional flow equations, Shi *et al.* (2022) assumed top–bottom symmetry in order to focus on important characteristics of non-axisymmetric drainage.

It should be noted that although surface bubbles serve as motivation for this study, flow in the film of a surface bubble cap may not be in the extensional flow regime. When shear stress increases in an otherwise free thin liquid film, e.g. by imposing a stronger surface tension gradient, the flow transitions (Champougny *et al.* 2015; Atasi *et al.* 2020) from the extensional flow regime, where the flow profile is plug-like, to the shear flow regime, where the flow profile is nearly parabolic (see figure 1). In particular, for surface bubbles, there are cases where the extensional flow regime is considered (Debrégeas, De Gennes & Brochard-Wyart 1998; Howell 1999; Shi *et al.* 2022; Bartlett *et al.* 2023), cases in which the shear flow regime is considered (Lhuissier & Villermaux 2012), and cases where both the extensional flow and shear flow regimes are considered (Champougny *et al.* 2016; Atasi *et al.* 2020; Miguet *et al.* 2020). For example, extensional flow is usually only considered for surface bubbles with drainage at low Reynolds number (Debrégeas *et al.* 1998; Nguyen *et al.* 2013); such a regime is of interest in industry and volcanology. Thus, the examples provided in §§ 4 and 5 should be seen as a fundamental study in liquid film dynamics rather than directly representing the film flow of any given surface bubble cap.

1.2. Outline of the paper

The paper is structured as follows. In § 2, the governing Navier–Stokes equations with corresponding boundary conditions are given. Then, in § 3, we give the asymmetric thin-film equations, including Marangoni effects, using an asymptotic expansion strategy from previous works (Howell 1996; Breward 1999), where the resulting equations extend equations already given by these authors. In §§ 4 and 5, we consider the example of the deposition of insoluble surfactants on one side of a liquid film. Specifically, in § 4, the liquid film is otherwise at rest and in § 5, the liquid film is otherwise uniformly thinning with a constant extension rate. We consider the case of low-Reynolds-number motions, $Re \ll 1$; see Appendix C for a brief discussion on including inertia.

1.3. Main results of the paper

The main results of the paper are as follows. First, analytical extensions to prior work is given for the relevant thin-film equations. For the surfactant deposition problem,

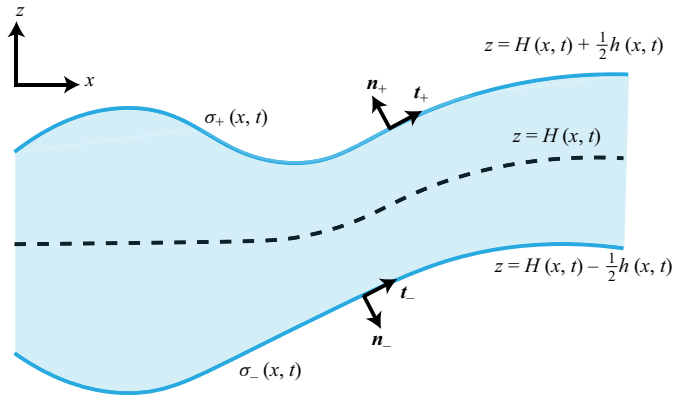


Figure 2. Schematic of a thin film with curved centreline $H(x, t)$ and thickness $h(x, t)$ (the x axis is in the horizontal direction, the z axis is in the vertical direction and t is time). The top surface of the film is given by $z = H(x, t) + \frac{1}{2}h(x, t)$ and the bottom surface of the film is given by $z = H(x, t) - \frac{1}{2}h(x, t)$. The outward normal of the top/bottom surface is denoted \mathbf{n}_{\pm} and the tangential vector (in the direction of increasing x) on the top/bottom surface is denoted \mathbf{t}_{\pm} . Surface tension at the top/bottom of the sheet is given by $\sigma_{\pm}(x, t)$.

analytical progress is made via transforming to Lagrangian coordinates, which allows us to (a) describe the evolution of the sheet, (b) discuss the effects of the shape of surfactant isotherms and (c) to discuss the possibility that satellite drops may be formed from pinching via Marangoni effects, such as when the initial surfactant isotherm has a double maximum.

2. Governing equations and boundary conditions

We consider an incompressible, two-dimensional Newtonian film (viscosity μ , density ρ) with the horizontal direction given by the x axis and the vertical direction given by the z axis. The top surface of the film is given by $z = H(x, t) + \frac{1}{2}h(x, t)$ and the bottom surface of the film is given by $z = H(x, t) - \frac{1}{2}h(x, t)$ (see figure 2). We assume that the fluid of the thin film is not coupled to the surrounding fluid; typically, the thin film is surrounded by air otherwise at rest.

Let $\epsilon := \mathcal{H}/\mathcal{L}$ be the aspect ratio between the characteristic vertical scale \mathcal{H} , e.g. the film thickness, and horizontal scale \mathcal{L} , e.g. a typical wavelength of a perturbation. Assume that $\epsilon \ll 1$, i.e. a thin film. The velocity field is denoted by (u, w) where u is the horizontal velocity and w is the vertical velocity. As we focus on the influence of asymmetries, we consider variable surface tension fields on the top and bottom interfaces, given by $\sigma_+(x, t)$ and $\sigma_-(x, t)$, respectively.

We consider the extensional flow regime $u(x, z, t) \approx u(x, t)$ and $p(x, z, t) \approx p(x, t)$, where the necessary conditions are given in § 3.2. The extensional flow regime is considered so that a one-dimensional description can be obtained formally, as is common in the thin-film literature (e.g. De Wit *et al.* 1994; Howell 1996; Breward 1999; Timmermans & Lister 2002; Bowen & Tilley 2013; Kitavtsev *et al.* 2018).

In order to close the equations, the surface tension $\sigma(x, t)$ must be given in terms of other variables in the system. For example (see § 4), the surface tension could be given in terms of a surfactant field $\Gamma(x, t)$, which in turn will have its own transport equation (Stone 1990). Another common scenario is when the surface tension is coupled to a temperature field (e.g. Bowen & Tilley 2013; Kitavtsev *et al.* 2018).

Asymmetric Marangoni flow

The two-dimensional continuity and Navier–Stokes equations apply to the fluid between $H - \frac{1}{2}h \leq z \leq H + \frac{1}{2}h$,

$$\frac{\partial u}{\partial x} + \frac{\partial w}{\partial z} = 0, \tag{2.1}$$

$$\rho \left(\frac{\partial u}{\partial t} + u \frac{\partial u}{\partial x} + w \frac{\partial u}{\partial z} \right) = -\frac{\partial p}{\partial x} + \mu \left(\frac{\partial^2 u}{\partial x^2} + \frac{\partial^2 u}{\partial z^2} \right), \tag{2.2}$$

$$\rho \left(\frac{\partial w}{\partial t} + u \frac{\partial w}{\partial x} + w \frac{\partial w}{\partial z} \right) = -\frac{\partial p}{\partial z} + \mu \left(\frac{\partial^2 w}{\partial x^2} + \frac{\partial^2 w}{\partial z^2} \right). \tag{2.3}$$

The outward normals of the top and bottom surfaces are denoted, respectively, by \mathbf{n}_\pm and the corresponding unit tangent vectors (in the direction of increasing x) are denoted, respectively, by \mathbf{t}_\pm (see figure 2). For each of the two surfaces, $z = H(x, t) \pm \frac{1}{2}h(x, t)$, we have one kinematic boundary condition and two dynamic boundary conditions. For notational convenience, let $z^\pm := H(x, t) \pm \frac{1}{2}h(x, t)$. The kinematic boundary conditions at the top and bottom surfaces, $z = z^\pm$, are given by

$$w|_{z=z^\pm} = \left(\frac{\partial H}{\partial t} \pm \frac{1}{2} \frac{\partial h}{\partial t} \right) + u|_{z=z^\pm} \left(\frac{\partial H}{\partial x} \pm \frac{1}{2} \frac{\partial h}{\partial x} \right). \tag{2.4}$$

Consider the \mathbf{n}_\pm and \mathbf{t}_\pm directions. Denote the curvatures of the surfaces by κ_\pm . The normal and tangential stress boundary conditions at the top and bottom surfaces, $z = z^\pm$ are given, respectively, by the two equations

$$\sigma_\pm \kappa_\pm = \left(p - \mu \frac{2 \left(\frac{\partial H}{\partial x} \pm \frac{1}{2} \frac{\partial h}{\partial x} \right)^2}{1 + \left(\frac{\partial H}{\partial x} \pm \frac{1}{2} \frac{\partial h}{\partial x} \right)^2} \frac{\partial u}{\partial x} + \mu \frac{2 \left(\frac{\partial H}{\partial x} \pm \frac{1}{2} \frac{\partial h}{\partial x} \right)}{1 + \left(\frac{\partial H}{\partial x} \pm \frac{1}{2} \frac{\partial h}{\partial x} \right)^2} \left(\frac{\partial u}{\partial z} + \frac{\partial w}{\partial x} \right) - \mu \frac{2}{1 + \left(\frac{\partial H}{\partial x} \pm \frac{1}{2} \frac{\partial h}{\partial x} \right)^2} \frac{\partial w}{\partial z} \right) \Bigg|_{z=z^\pm}, \tag{2.5}$$

$$\frac{\partial \sigma_\pm}{\partial x} = \left(\pm \mu \frac{2 \left(\frac{\partial H}{\partial x} \pm \frac{1}{2} \frac{\partial h}{\partial x} \right)}{\sqrt{1 + \left(\frac{\partial H}{\partial x} \pm \frac{1}{2} \frac{\partial h}{\partial x} \right)^2}} \left(\frac{\partial w}{\partial z} - \frac{\partial u}{\partial x} \right) \pm \mu \frac{1 - \left(\frac{\partial H}{\partial x} \pm \frac{1}{2} \frac{\partial h}{\partial x} \right)^2}{\sqrt{1 + \left(\frac{\partial H}{\partial x} \pm \frac{1}{2} \frac{\partial h}{\partial x} \right)^2}} \left(\frac{\partial u}{\partial z} + \frac{\partial w}{\partial x} \right) \right) \Bigg|_{z=z^\pm}, \tag{2.6}$$

where the curvatures κ_{\pm} of the top and bottom surfaces, $z = z^{\pm}$, are given by

$$\kappa_{\pm} = \frac{\mp \frac{\partial^2 H}{\partial x^2} - \frac{1}{2} \frac{\partial^2 h}{\partial x^2}}{\left(1 + \left(\frac{\partial H}{\partial x} \pm \frac{1}{2} \frac{\partial h}{\partial x}\right)^2\right)^{3/2}}. \tag{2.7}$$

3. Asymmetric thin-film equations in extensional flow

In this section, we provide a derivation, using an asymptotic expansion in the small aspect ratio ϵ , to obtain the leading-order non-symmetric thin-film equations for extensional flow. In particular, we allow for top–bottom asymmetry, which leads to a curved centreline. The full details of the derivation are provided in the supplementary material available at <https://doi.org/10.1017/jfm.2024.501> for completeness, while here we provide a summary of the key ideas.

The derivation is analogous to that of Howell (1996) and Breward (1999). There are slight differences in the terms considered since Howell (1996) does not consider Marangoni effects and Breward (1999) does not consider inertia (and time evolution of H and \bar{w}). Thus, the resulting equations in this paper are extensions to previous work (see § 3.5). In particular, the inclusion of the inertial and Marangoni effects are important for the examples given in §§ 4 and 5. The shortened derivation has been included for completeness.

3.1. Non-dimensionalisation

We first non-dimensionalise the equations according to

$$\left. \begin{aligned} x = \mathcal{L}\tilde{x}, \quad u = \mathcal{U}\tilde{u}, \quad H = \epsilon\mathcal{L}\tilde{H}, \quad t = \frac{\mathcal{L}}{\mathcal{U}}\tilde{t}, \quad y = \epsilon\mathcal{L}\tilde{y}, \quad w = \epsilon\mathcal{U}\tilde{w}, \\ h = \epsilon\mathcal{L}\tilde{h}, \quad p = \frac{\mu\mathcal{U}}{\mathcal{L}}\tilde{p}, \quad \sigma = \Sigma + (\Delta\Sigma)\tilde{\sigma}, \end{aligned} \right\} \tag{3.1}$$

where \mathcal{U} is some constant characteristic velocity, Σ is some constant characteristic surface tension and $\Delta\Sigma$ is a characteristic surface tension variation of interest in the problem. There are three dimensionless parameters: Reynolds number $Re = \rho\mathcal{U}\mathcal{L}/\mu$, Marangoni number $M = \Delta\Sigma/\epsilon\mu\mathcal{U}$ and capillary number $C = \epsilon\mu\mathcal{U}/\Sigma$. The parameter ϵ is included in the definition of M and C in a way such that (a) the later discussed thresholds for the extensional flow conditions are $O(1)$ (see (3.10) and (3.11)) and (b) the complete equations become independent of ϵ (see § 3.5). Note that in the non-dimensionalisation (3.1), we are considering timescales \mathcal{L}/\mathcal{U} (see § 4.7 for a discussion of shorter timescales). Henceforth, the tilde ($\tilde{}$) will be omitted.

3.1.1. Non-dimensional equations

The bulk equations (2.1), (2.2) and (2.3) in dimensionless form are

$$\frac{\partial u}{\partial x} + \frac{\partial w}{\partial z} = 0, \tag{3.2}$$

$$Re \left(\frac{\partial u}{\partial t} + u \frac{\partial u}{\partial x} + w \frac{\partial u}{\partial z} \right) = -\frac{\partial p}{\partial x} + \left(\frac{\partial^2 u}{\partial x^2} + \frac{1}{\epsilon^2} \frac{\partial^2 u}{\partial z^2} \right), \tag{3.3}$$

$$Re \left(\frac{\partial w}{\partial t} + u \frac{\partial w}{\partial x} + w \frac{\partial w}{\partial z} \right) = -\frac{1}{\epsilon^2} \frac{\partial p}{\partial z} + \left(\frac{\partial^2 w}{\partial x^2} + \frac{1}{\epsilon^2} \frac{\partial^2 w}{\partial z^2} \right). \tag{3.4}$$

Next, the kinematic boundary conditions (2.4) are given by

$$w|_{z=z^\pm} = \left(\frac{\partial H}{\partial t} \pm \frac{1}{2} \frac{\partial h}{\partial t} \right) + u|_{z=z^\pm} \left(\frac{\partial H}{\partial x} \pm \frac{1}{2} \frac{\partial h}{\partial x} \right). \tag{3.5}$$

With the non-dimensionalisation, the normal and tangential stress boundary conditions (2.5) and (2.6) are given by

$$\begin{aligned} \frac{\epsilon^2}{C} (1 + MC\sigma_\pm) \kappa_\pm = & \left(p - \frac{2 \left(\frac{\partial H}{\partial x} \pm \frac{1}{2} \frac{\partial h}{\partial x} \right)^2}{1 + \epsilon^2 \left(\frac{\partial H}{\partial x} \pm \frac{1}{2} \frac{\partial h}{\partial x} \right)^2} \epsilon^2 \frac{\partial u}{\partial x} \right. \\ & \left. + \frac{2 \left(\frac{\partial H}{\partial x} \pm \frac{1}{2} \frac{\partial h}{\partial x} \right)}{1 + \epsilon^2 \left(\frac{\partial H}{\partial x} \pm \frac{1}{2} \frac{\partial h}{\partial x} \right)^2} \left(\frac{\partial u}{\partial z} + \epsilon^2 \frac{\partial w}{\partial x} \right) - \frac{2}{1 + \epsilon^2 \left(\frac{\partial H}{\partial x} \pm \frac{1}{2} \frac{\partial h}{\partial x} \right)^2} \frac{\partial w}{\partial z} \right) \Bigg|_{z=z^\pm} \end{aligned} \tag{3.6}$$

and

$$\begin{aligned} \epsilon^2 M \frac{\partial \sigma_\pm}{\partial x} = & \left(\pm \frac{2 \left(\frac{\partial H}{\partial x} \pm \frac{1}{2} \frac{\partial h}{\partial x} \right) \epsilon^2}{\sqrt{1 + \epsilon^2 \left(\frac{\partial H}{\partial x} \pm \frac{1}{2} \frac{\partial h}{\partial x} \right)^2}} \left(\frac{\partial w}{\partial z} - \frac{\partial u}{\partial x} \right) \right. \\ & \left. \pm \frac{1 - \epsilon^2 \left(\frac{\partial H}{\partial x} \pm \frac{1}{2} \frac{\partial h}{\partial x} \right)^2}{\sqrt{1 + \epsilon^2 \left(\frac{\partial H}{\partial x} \pm \frac{1}{2} \frac{\partial h}{\partial x} \right)^2}} \left(\frac{\partial u}{\partial z} + \epsilon^2 \frac{\partial w}{\partial x} \right) \right) \Bigg|_{z=z^\pm}, \end{aligned} \tag{3.7}$$

where the curvatures κ_\pm (2.7) are given by

$$\kappa_\pm = \frac{\mp \frac{\partial^2 H}{\partial x^2} - \frac{1}{2} \frac{\partial^2 h}{\partial x^2}}{\left(1 + \epsilon^2 \left(\frac{\partial H}{\partial x} \pm \frac{1}{2} \frac{\partial h}{\partial x} \right)^2 \right)^{3/2}}. \tag{3.8}$$

These equations involve four non-dimensional parameters, ϵ , Re , M and C .

3.2. Conditions for extensional flow

In order to have extensional flow, i.e. $u(x, z, t) \approx u(x, t)$ and $p(x, z, t) \approx p(x, t)$ to leading order in ϵ , we require three conditions. The first condition is that inertia does not play a

dominant role:

$$\text{Re} \left(\frac{\partial u}{\partial t} + u \frac{\partial u}{\partial x} + w \frac{\partial u}{\partial z} \right) = O(1) \text{ or less.} \tag{3.9}$$

Starting with (3.3), this condition yields $\partial^2 u / \partial z^2 = 0$ to leading order; see (3.13). The second condition is that the tangential stress is not too large:

$$M \frac{\partial \sigma_{\pm}}{\partial x} = O(1) \text{ or less.} \tag{3.10}$$

This condition yields the horizontal velocity field $u(x, z, t) \approx u(x, t)$; see (3.14). The third condition is that the capillary pressure due to surface tension is not too large:

$$\frac{1}{C} (1 + MC\sigma_{\pm}) \kappa_{\pm} = O(1) \text{ or less.} \tag{3.11}$$

This condition yields the pressure field $p(x, z, t) \approx p(x, t)$; see (3.19).

The first two conditions (3.9) and (3.10) are commonly discussed elsewhere (De Wit *et al.* 1994; Breward 1999; Timmermans & Lister 2002; Bowen & Tilley 2013; Kitavtsev *et al.* 2018). The third condition (3.11) has also been mentioned (Howell 1996; Breward 1999). In the case of symmetry ($\sigma = \sigma_{\pm}$, $\kappa = \kappa_{\pm}$), the right-hand side of (3.11) may be replaced with the phrase ‘ $O(\epsilon^{-2})$ or less’ (see Appendix A). Thus, (3.11) is a condition that becomes more strict due to the asymmetry of interest.

3.3. Leading-order expansion

We expand the horizontal velocity as

$$u(x, z, t) = u_0(x, z, t) + \epsilon^2 u_1(x, z, t) + \dots \tag{3.12}$$

and consider analogous expansions for w, H, h , and p . We consider the leading-order expansion first where we ignore relative errors of order $O(\epsilon^2)$. The horizontal momentum equation (3.3) using the first condition (3.9) gives

$$\frac{\partial^2 u_0}{\partial z^2} = 0. \tag{3.13}$$

The tangential boundary conditions (3.7), after using the second condition (3.10), give

$$\left. \frac{\partial u_0}{\partial z} \right|_{z=z^{\pm}} = 0, \tag{3.14}$$

which shows that the leading-order horizontal velocity is independent of z ,

$$u_0 = u_0(x, t). \tag{3.15}$$

Then, continuity (3.2) gives

$$w_0 = \bar{w}(x, t) - (z - H_0) \frac{\partial u_0}{\partial x}, \tag{3.16}$$

where \bar{w} denotes the average of w in the vertical direction ($\bar{f} := (1/h) \int_{z^-}^{z^+} f(x, z, t) dz$).

Asymmetric Marangoni flow

Next, turning to the vertical momentum equation (3.4) and using (3.9) gives

$$\frac{\partial p_0}{\partial z} = \frac{\partial^2 w_0}{\partial z^2}, \quad (3.17)$$

which upon substitution of (3.16) yields

$$p_0 = p_0(x, t). \quad (3.18)$$

Then, considering the normal stress boundary conditions (3.6), along with continuity (3.2), gives

$$0 = p_0 + 2 \frac{\partial u_0}{\partial x}. \quad (3.19)$$

Finally, with the kinematic boundary conditions (3.5), and using (3.16) for w_0 , we find

$$\bar{w} \mp \frac{1}{2} h_0 u_0 = \left(\frac{\partial H_0}{\partial t} \pm \frac{1}{2} \frac{\partial h_0}{\partial t} \right) + u_0 \left(\frac{\partial H_0}{\partial x} \pm \frac{1}{2} \frac{\partial h_0}{\partial x} \right), \quad (3.20)$$

which can be added and subtracted to find

$$\frac{\partial H_0}{\partial t} + u_0 \frac{\partial H_0}{\partial x} = \bar{w} \quad (3.21)$$

and

$$\frac{\partial h_0}{\partial t} + \frac{\partial}{\partial x} (u_0 h_0) = 0. \quad (3.22)$$

3.4. Next-order expansion

We can follow the same steps as in § 3.3 for the $O(\epsilon^2)$ equations. The details are provided in the supplementary material. Explicitly, we consider the horizontal momentum equation and the tangential stress conditions to deduce

$$Reh_0 \left(\frac{\partial u_0}{\partial t} + u_0 \frac{\partial u_0}{\partial x} \right) = M \left(\frac{\partial \sigma_+}{\partial x} + \frac{\partial \sigma_-}{\partial x} \right) + 4 \frac{\partial}{\partial x} \left(h_0 \frac{\partial u_0}{\partial x} \right). \quad (3.23)$$

Similarly, the vertical momentum equation and the normal stress conditions lead to

$$\begin{aligned} Reh_0 \left(\frac{\partial \bar{w}}{\partial t} + u_0 \frac{\partial \bar{w}}{\partial x} \right) &= \frac{1}{2} M \frac{\partial^2}{\partial x^2} (h_0(\sigma_+ - \sigma_-)) + \frac{\partial}{\partial x} \left(\frac{\partial H_0}{\partial x} \left(\frac{2}{C} + M(\sigma_+ + \sigma_-) \right) \right) \\ &+ 4 \frac{\partial}{\partial x} \left(h_0 \frac{\partial H_0}{\partial x} \frac{\partial u_0}{\partial x} \right). \end{aligned} \quad (3.24)$$

3.5. Complete equations

In this subsection, the complete non-dimensional equations are given for clarity. From this point onwards, we refer to h_0 as h , H_0 as H and u_0 as \bar{u} . Then, the evolution equations for

the dimensional counterparts h, H, \bar{u} and \bar{w} are given by

$$\frac{\partial h}{\partial t} + \frac{\partial}{\partial x}(\bar{u}h) = 0, \tag{3.25}$$

$$\frac{\partial H}{\partial t} + \bar{u}\frac{\partial H}{\partial x} = \bar{w}, \tag{3.26}$$

$$Reh \left(\frac{\partial \bar{u}}{\partial t} + \bar{u}\frac{\partial \bar{u}}{\partial x} \right) = M \left(\frac{\partial \sigma_+}{\partial x} + \frac{\partial \sigma_-}{\partial x} \right) + 4\frac{\partial}{\partial x} \left(h\frac{\partial \bar{u}}{\partial x} \right), \tag{3.27}$$

$$Reh \left(\frac{\partial \bar{w}}{\partial t} + \bar{u}\frac{\partial \bar{w}}{\partial x} \right) = \frac{1}{2}M\frac{\partial^2}{\partial x^2} (h(\sigma_+ - \sigma_-)) + \frac{\partial}{\partial x} \left(\frac{\partial H}{\partial x} \left(\frac{2}{C} + M(\sigma_+ + \sigma_-) \right) \right) + 4\frac{\partial}{\partial x} \left(h\frac{\partial H}{\partial x}\frac{\partial \bar{u}}{\partial x} \right). \tag{3.28}$$

In the above equations, the dynamics depend only on Re, M and C . In the symmetric case $H = 0, \sigma_{\pm} = \sigma$ and $\bar{w} = 0$, we recover equations already familiar in the literature (De Wit *et al.* 1994). The capillary pressure term $\frac{1}{2}(\epsilon^2/C)h(\partial^3 h/\partial x^3)$ does not appear in the above equations since we consider $C = O(1)$ or greater; see Appendix A.

Equations (3.25) and (3.26) have been given in the literature previously (Howell 1996; Breward 1999). In addition, (3.27) was given by Breward (1999), though inertia was omitted, and (3.28) with $\sigma_+ = \sigma_-$ constant was given by Howell (1996). To the best of the authors’ knowledge, the evolution equation (3.28) for \bar{w} with Marangoni effects has not been considered so far in the literature. In the example of surfactant deposition on a sheet, which we consider in §§ 4 and 5, asymmetric surface tension variations are considered in (3.28) in order to solve for the resulting centreline deformation H .

Before proceeding further, we provide intuition for (3.25)–(3.28). The evolution equation for h (3.25) expresses conservation of mass. The evolution equation for H (3.26) can be regarded as $DH/Dt = \bar{w}$ where D/Dt is the material derivative. Thus, the evolution equation for H indicates that the centreline moves with the mean vertical flow. For the horizontal momentum equation (3.27), the left-hand side is inertia, the first term of the right-hand side is from the Marangoni force and the second term of the right-hand side is viscous stresses (sometimes referred to as ‘Trouton viscosity’). The vertical momentum equation (3.28) can be discussed in a similar way.

4. Thinning, rupture and bending of a liquid sheet due to an asymmetric deposition of insoluble surfactants

In this section, we consider the localised deposition of insoluble surfactants onto the top, $z = H + \frac{1}{2}h$, of a sheet of initial uniform thickness $h = h_I$ otherwise at rest (the bottom, $z = H - \frac{1}{2}h$, remains clean). Without surfactants, we assume that $\sigma_{\pm} = \Sigma = \text{constant}$. A gradient of surface tension is created as result of the surfactants and Marangoni-driven flow occurs. Since we consider surface tension variations due to surfactants, we must use a surface tension isotherm (Manikantan & Squires 2020) $\sigma = \sigma(\Gamma)$, such as the Langmuir isotherm. We show that due to top–bottom asymmetry, the centreline H will evolve (see (4.8)), i.e. bending will occur. Since the sheet starts at rest, the flow requires some time before reaching the extensional flow regime. For $Re = O(1)$ or less, this short time may be safely ignored (see Appendix B).

Asymmetric Marangoni flow

We assume that the Péclet number, defined by $\mathcal{L}\Delta\Sigma/\epsilon\mu D$ (see § 4.1) is large enough such that diffusion may be ignored. We consider $Re \ll 1$. In Appendix C, we discuss the effect of including some inertia up to $Re = O(1)$.

A related set-up was considered experimentally (Néel & Villermaux 2018), where rupture of a liquid sheet could be achieved due to Marangoni flow arising from the deposition of surfactants. It should, however, be noted that the set-up considered in the experiment yields $Re \gg 1$. In contrast, this section considers $Re \ll 1$. There are also many studies considering numerically and/or analytically the thinning of a symmetric two-dimensional sheet due to Marangoni effects in an extensional flow regime (e.g. De Wit *et al.* 1994; Bowen & Tilley 2013; Kitavtsev *et al.* 2018; Wee, Wagoner & Basaran 2022).

A physical example where the equations would be valid is as follows. Consider a glycerol film ($\rho \approx 10^3 \text{ kg m}^{-3}$, $\mu \approx 1 \text{ Pa s}$, $\Sigma \approx 0.06 \text{ N m}^{-1}$) with $\mathcal{L} = 100 \mu\text{m}$, $\epsilon = 0.1$ and $\Delta\Sigma/\Sigma = 0.5$. The values represent, for example, the deposition of a drop of surfactants over a scale of $100 \mu\text{m}$ onto a sheet of thickness $10 \mu\text{m}$ and assumes that the drop changes the surface tension by 50%. Then, $Re = \rho\mathcal{L}\Delta\Sigma/\epsilon\mu^2 \approx 0.03$ (see § 4.1) so $Re \ll 1$, $C = O(1)$ and the approach given in the following is applicable.

For the figures in this section, we pick a particular choice of the capillary number, $C = 0.5$. Other choices for C with $C = O(1)$ or greater would have been valid also. The effect of changing C is only a change in the prefactor of H and \bar{w} (see (4.8) and (4.14)).

4.1. Non-dimensional equations

Since there is no background flow, we note that \mathcal{U} is set by the tangential Marangoni stress. Thus, we take $\mathcal{U} = \Delta\Sigma/\epsilon\mu$ (in other words, take $M = 1$). Then, $Re = \rho\mathcal{L}\Delta\Sigma/\epsilon\mu^2$, $C = \Delta\Sigma/\Sigma$. We define $\epsilon = h_l/\mathcal{L}$. In addition, non-dimensionalise the surfactant concentration with a characteristic surfactant concentration Γ_c . Explicitly,

$$\left. \begin{aligned} x = \mathcal{L}\tilde{x}, \quad u = \frac{\Delta\Sigma}{\epsilon\mu}\tilde{u}, \quad H = \epsilon\mathcal{L}\tilde{H}, \quad t = \frac{\epsilon\mu\mathcal{L}}{\Delta\Sigma}\tilde{t}, \quad y = \epsilon\mathcal{L}\tilde{y}, \quad w = \frac{\Delta\Sigma}{\mu}\tilde{w}, \\ h = \epsilon\mathcal{L}\tilde{h}, \quad \sigma = \Sigma + \Delta\Sigma\tilde{\sigma}, \quad \Gamma = \Gamma_c\tilde{\Gamma}. \end{aligned} \right\} \quad (4.1)$$

Note that, by definition, $\tilde{\sigma}(\Gamma = 0) = 0$. Again, the tilde ($\tilde{}$) is dropped. We consider $C = O(1)$ or larger so that we have extensional flow (see § 3.2). The horizontal length scale \mathcal{L} is given by the width of variation of the initial surfactant concentration. For example a Gaussian initial surfactant distribution Γ_l is represented as $\Gamma_l \propto e^{-x^2}$.

Equations (3.25) and (3.26) are as before. Since $Re \ll 1$, the inertia terms of (3.27) and (3.28) can be neglected to deduce, respectively, quasi-static balances of horizontal momentum and vertical momentum given by

$$0 = \left(\frac{\partial\sigma_+}{\partial x} + \frac{\partial\sigma_-}{\partial x} \right) + 4 \frac{\partial}{\partial x} \left(h \frac{\partial\bar{u}}{\partial x} \right), \quad (4.2)$$

$$\begin{aligned} 0 = \frac{1}{2} \frac{\partial^2}{\partial x^2} (h(\sigma_+ - \sigma_-)) + \frac{\partial}{\partial x} \left(\frac{\partial H}{\partial x} \left(\frac{2}{C} + (\sigma_+ + \sigma_-) \right) \right) \\ + 4 \frac{\partial}{\partial x} \left(h \frac{\partial H}{\partial x} \frac{\partial\bar{u}}{\partial x} \right). \end{aligned} \quad (4.3)$$

It should be noted that there is now a single parameter (C) remaining, which as noted at the beginning of the section, only changes the prefactor of H and \bar{w} . The quasi-static balance

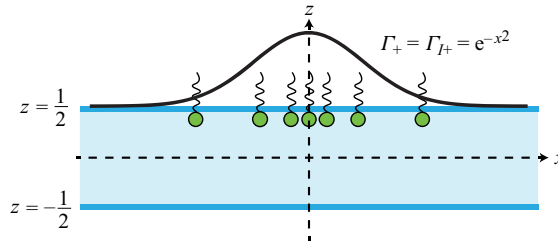


Figure 3. Initial set-up considered in §4.4. An initial Gaussian surfactant distribution $\Gamma_{I+}(x) = e^{-x^2}$, $\Gamma_{I-}(x) = 0$ is deposited onto the top of a uniform sheet at rest $-\frac{1}{2} \leq z \leq \frac{1}{2}$ at $t = 0$. The horizontal direction is given by the x axis and the vertical direction is given by the z axis. See (4.1) for the non-dimensionalisation.

occurs on the dimensional timescale given by $t_{qs} := \epsilon\mu\mathcal{L}/\Delta\Sigma$. The system adjusts itself from the initial condition to the quasi-static balance on dimensional timescales much shorter than t_{qs} and these details are discussed in §4.7, where inertia is important. Since diffusion of surfactants is neglected, the equations for surfactant concentration at the top and bottom surfaces, $\Gamma_{\pm}(x, t)$, are given to leading order, correct up to $O(\epsilon^2)$ errors, by

$$\frac{\partial\Gamma_{\pm}}{\partial t} + \frac{\partial}{\partial x}(\bar{u}\Gamma_{\pm}) = 0. \tag{4.4}$$

If diffusion is not ignored, the term $(\epsilon\mu D/\mathcal{L}\Delta\Sigma)(\partial^2\Gamma_{\pm}/\partial x^2)$ (diffusion coefficient D) appears on the right-hand side of (4.4). In neglecting diffusion of surfactants, we are assuming that the Péclet number $\mathcal{L}\Delta\Sigma/\epsilon\mu D$ is sufficiently large. Neglecting the influence of diffusion is also physically motivated. Upon taking surfactant diffusivity $D = 10^{-10} \text{ m}^2 \text{ s}^{-1}$, along with the values quoted at the beginning of the section ($\Delta\Sigma = 0.006 \text{ N m}^{-1}$, $\mathcal{L} = 100 \text{ }\mu\text{m}$, $\mu = 1 \text{ Pa s}$, $\epsilon = 0.1$) and the Péclet number $\mathcal{L}\Delta\Sigma/\epsilon\mu D \approx 6 \times 10^4 \gg 1$.

4.2. Initial and boundary conditions

For the initial conditions, we consider a uniform sheet otherwise at rest, along with some initial surfactant distribution $\Gamma_{I\pm}(x)$ where $\Gamma_{I\pm} \rightarrow 0$ as $x \rightarrow \pm\infty$. Far field conditions are taken for the boundary condition. See figure 3 for a particular example where $\Gamma_{I+} = e^{-x^2}$ and $\Gamma_{I-} = 0$, which is considered in §4.4. Explicitly,

$$h = 1, H = 0, \bar{u} = 0, \bar{w} = 0, \Gamma_{\pm} = \Gamma_{I\pm} \quad \text{at } t = 0 \tag{4.5}$$

and

$$h = 1, H = 0, \frac{\partial\bar{u}}{\partial x} = 0, \bar{w} = 0, \Gamma_{\pm} = 0 \quad \text{at } x = \pm\infty. \tag{4.6}$$

4.3. Lagrangian coordinates

Lagrangian coordinates are useful in discussing the inertialess evolution of liquid sheets and liquid threads (Eggers & Fontelos 2015). In this problem, using Lagrangian coordinates allows us to deduce physical conclusions for a general surfactant isotherm $\sigma = \sigma(\Gamma)$.

Before switching to Lagrangian coordinates, we first do some algebra. Integrating the horizontal momentum equation (4.2) with respect to x , and using boundary conditions

(4.6), gives

$$\frac{\partial \bar{u}}{\partial x} = -\frac{1}{4h(x, t)} (\sigma(\Gamma_+(x, t)) + \sigma(\Gamma_-(x, t))), \quad (4.7)$$

which can be substituted into (4.3) and integrated twice with respect to x to deduce an analytic expression for the centreline H shape given by

$$H(x, t) = -\frac{C}{4} h(\sigma(\Gamma_+(x, t)) - \sigma(\Gamma_-(x, t))). \quad (4.8)$$

Denote the Lagrangian coordinates by the initial material spatial coordinate s defined so that $x = x(s, t)$ with $s = x(s, 0)$. At initial time $t = 0$, the Eulerian and Lagrangian coordinates therefore agree. Denoting the Lagrangian time derivative by D/Dt , (3.25) and (4.4) give

$$\left. \frac{Dh}{Dt} \right|_{(s,t)} = -h \left. \frac{\partial \bar{u}}{\partial x} \right|_{(x(s,t),t)} \quad (4.9)$$

and

$$\left. \frac{D\Gamma_{\pm}}{Dt} \right|_{(s,t)} = -\Gamma_{\pm} \left. \frac{\partial \bar{u}}{\partial x} \right|_{(x(s,t),t)}, \quad (4.10)$$

which gives that

$$\left. \frac{D}{Dt} \left(\frac{\Gamma_{\pm}}{h} \right) \right|_{(s,t)} = \frac{1}{h^2} \left(-\Gamma_{\pm} h \left. \frac{\partial \bar{u}}{\partial x} \right|_{(x(s,t),t)} + h \Gamma_{\pm} \left. \frac{\partial \bar{u}}{\partial x} \right|_{(x(s,t),t)} \right) = 0. \quad (4.11)$$

Thus, in Lagrangian coordinates,

$$\Gamma_{\pm}(s, t) = \Gamma_{\pm}(s)h(s, t); \quad (4.12)$$

note that (4.12) would not have been deduced if diffusion was included. The result makes sense physically by considering a material volume of initial width Δs . For example, halving h would mean that the width of the volume has doubled, the interfacial area along a surface doubles, and thus in the case of no diffusion, surfactant concentration would be halved. The conservation equation (4.11) has been discussed by Chomaz (2001). Finally, (4.7) and (4.12) can be substituted into (4.9) to deduce that

$$\left. \frac{Dh}{Dt} \right|_{(s,t)} = \frac{1}{4} (\sigma(\Gamma_{I+}(s)h(s, t)) + \sigma(\Gamma_{I-}(s)h(s, t))). \quad (4.13)$$

Equation (4.13) is a first-order ordinary differential equation (ODE) for h in Lagrangian coordinates at a given point s with the initial condition $h = 1$. An expression for \bar{w} can also be found in terms of h from

$$\bar{w}(s, t) = \left. \frac{DH}{Dt} \right|_{(s,t)}, \quad (4.14)$$

which directly follows from (3.26). Thus, given a surfactant isotherm $\sigma = \sigma(\Gamma)$, one only needs to solve a single ODE, (4.13), to find the evolution of h following a given Lagrangian coordinate (s, t) , which in turn can be used to find the evolution of H , \bar{u} , \bar{w} , and Γ_{\pm} via, respectively, (4.8), (4.7), (4.14) and (4.12). Finally, the Lagrangian and Eulerian coordinates are related via

$$\left. \frac{\partial x}{\partial s} \right|_{(s,t)} = \frac{1}{h(s, t)}, \quad (4.15)$$

which can be deduced from standard arguments using conservation of mass (see Appendix D).

4.4. *Example: linear isotherm, Gaussian deposition on top*

In this subsection, we consider an example where the initial surfactant distribution given by $\Gamma_+(s) = e^{-s^2}$ and $\Gamma_-(s) = 0$ and the surface tension isotherm is linear $\sigma(\Gamma) = -\Gamma$ (see [figure 3](#) for the set-up). Then, we have

$$\left. \frac{Dh}{Dt} \right|_{(s,t)} = -K(s)h(s, t), \tag{4.16}$$

where $K(s) := \frac{1}{4}e^{-s^2}$. Using the initial condition $h(s, 0) = 1$, we have the analytic solution

$$h(s, t) = e^{-K(s)t}. \tag{4.17}$$

Equation (4.17) is the solution for h given the (3.25), (3.26), (3.27), (3.28), (4.5) and (4.6) with $\sigma(\Gamma) = -\Gamma$, $\Gamma_+(s) = e^{-s^2}$ and $\Gamma_-(s) = 0$. In turn, the solution for h given by (4.17) can be substituted into (4.8), (4.7), (4.14) and (4.12) to deduce equations for H , \bar{u} , \bar{w} and Γ_{\pm} via

$$H(s, t) = CK(s)e^{-2K(s)t}, \tag{4.18}$$

$$\bar{u}(s, t) = \int_0^s K(s')e^{K(s')t} ds', \tag{4.19}$$

$$\bar{w}(s, t) = -2CK^2(s)e^{-2K(s)t}, \tag{4.20}$$

$$\Gamma_+(s, t) = 4K(s)e^{-K(s)t} \quad \text{and} \quad \Gamma_-(s, t) = 0. \tag{4.21a,b}$$

The corresponding transformation into Eulerian coordinates is given by

$$x(s, t) = \int_0^s \frac{1}{h(s', t)} ds', \tag{4.22}$$

which follows from (4.15) and the symmetry condition $x(0, t) = 0$.

In particular, we can conclude from (4.13) that h does not pinch off in finite time. A point of caution is that as the thickness of the sheet tends towards rupture, other forces such as van der Waals forces become important. The rupture of a liquid film with van der Waals forces has been discussed elsewhere, both for the case without surfactants (Vaynblat, Lister & Witelski 2001) and with surfactants (Wee *et al.* 2022). In comparison, when the initial condition is a uniformly thinning sheet (see § 5.4), there is finite time pinch off even without van der Waals forces.

4.4.1. *Description of the solution*

Next, we give a description of the solution given by (4.17), (4.18), (4.19), (4.20) and (4.21a,b) in Eulerian coordinates to help gain intuition for the thinning and rupture of the sheet. For the figures in this section, we pick a particular choice of the capillary number, $C = 0.5$. Other choices for C with $C = O(1)$ or greater would have been valid also. The effect of changing C is only a change in the prefactor of H and \bar{w} (see (4.8) and (4.14)).

An example with $C = 0.5$ is given in [figure 4](#). In particular, [figure 4\(a\)](#) shows the bottom of the sheet $H - \frac{1}{2}h$, the centreline H , the top of the sheet $H + \frac{1}{2}h$ and the surfactant distribution Γ_+ at the initial time. By initial time, we mean $t = 0$ where a quasi-static balance has already been achieved and so, in particular, the centreline is bent (see §§ 4.1 and 4.7). [Figure 4\(b\)](#) shows the velocity profiles \bar{u} and \bar{w} at the initial time.

Asymmetric Marangoni flow

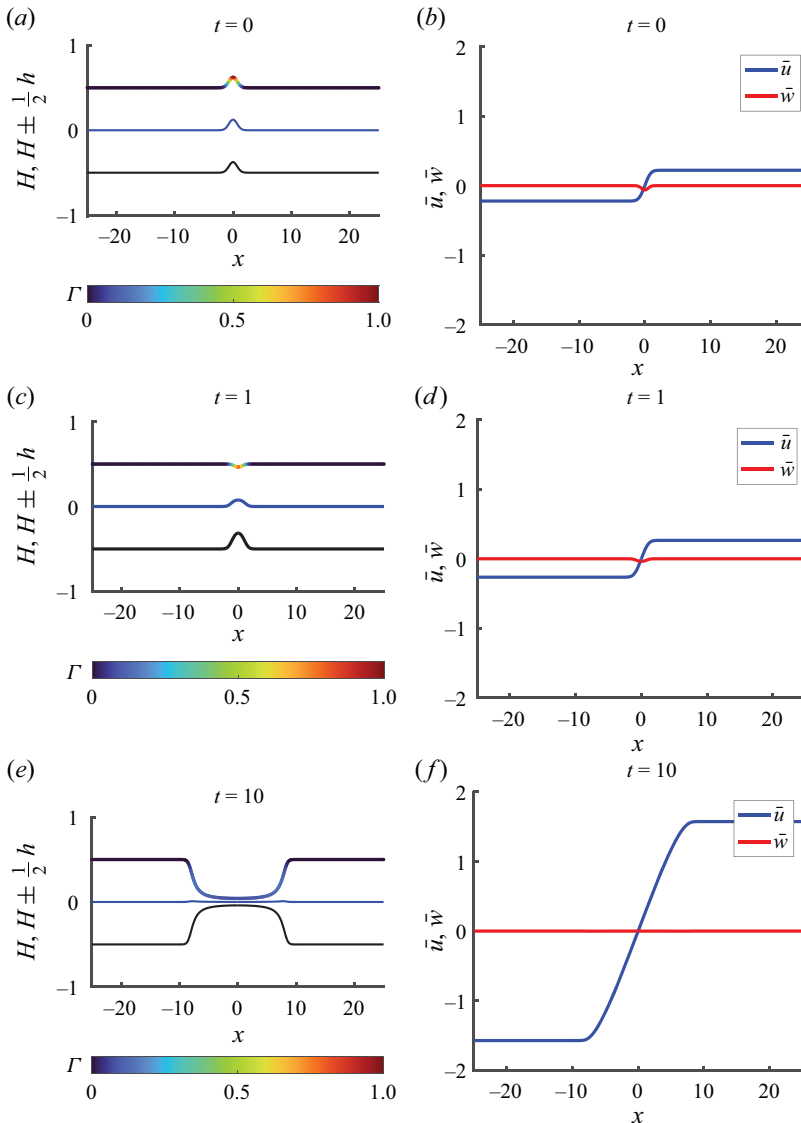


Figure 4. Plots of the space and time evolution of the thin-film dynamics, as given by (4.17), (4.22), (4.18), (4.19), (4.20) and (4.21a,b) for $C = 0.5$. The spatial variable x is in Eulerian coordinates. The three curves from bottom to top in (a) are $H - \frac{1}{2}h$ (black), H (blue) and $H + \frac{1}{2}h$ (coloured with surfactant concentration Γ) at the initial time and (b) shows the velocity profiles \bar{u} (blue) and \bar{w} (red) at the initial time. Similarly, (c,d) report the variables at $t = 1$ and (e,f) report the variables at $t = 10$. For the non-dimensionalisation, see (4.1).

Similarly, figure 4(c,d) report the variables at $t = 1$ and figure 4(e,f) report the variables at $t = 10$. The times $t = 1$ and 10 were chosen to represent mid and late times, respectively, for the thinning problem.

The non-uniform surfactant distribution means that there are Marangoni effects, where surfactants spread from a region of high concentration to low concentration (see figure 4a,c,e), since low concentration regions have higher surface tension. As result of the horizontal velocity \bar{u} induced by the spreading of surfactants, h decreases and the sheet thins as seen in figure 4(a,c,e).

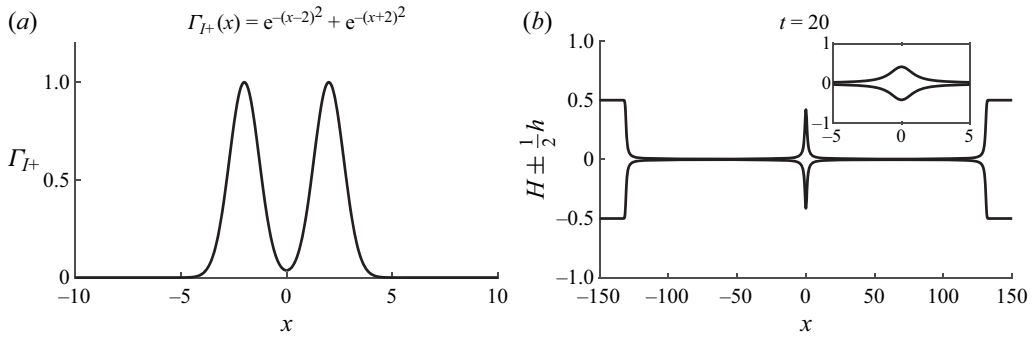


Figure 5. A deposition problem with initial surfactant concentration given by $\Gamma_{I+}(x) = e^{-(x-2)^2} + e^{-(x+2)^2}$, $\Gamma_{I-}(x) = 0$. (a) The initial surfactant concentration at the top surface Γ_{I+} . (b) The sheet profile $H \pm \frac{1}{2}h$ at $t = 20$, where the inset shows the sheet profile $H \pm \frac{1}{2}h$ near the satellite drop (included to illustrate the drop shape). In (b), the inset and the main figure have the same axes. The spatial variable x is in Eulerian coordinates. The isotherm chosen is $\sigma(\Gamma) = -\Gamma$ and the capillary parameter $C = 0.5$. For the non-dimensionalisation, see (4.1). A ‘satellite drop’ is formed around $x = 0$.

Since asymmetry has been accounted for, it is also possible to discuss the evolution of the centreline H and the vertical velocity \bar{w} . There is only non-uniform surface tension on the top of the sheet. Initially, the centreline H bends towards the top surface, which makes sense physically since the surface tension on the top surface is lower (the same fact can be seen from (4.8)). For the example shown in figure 4, the top of the sheet is pulled away from $x = 0$. As result, there is a region of negative \bar{w} around $x = 0$. Then, as time progresses, H reverts back towards the straight configuration at $z = 0$.

4.5. Example with a satellite drop: linear isotherm, double maximum

The example shown in § 4.4 considered a single maximum in the initial surfactant distribution. Another important example would be to consider multiple maxima. Continuing from § 4.4, we consider an example where the initial surfactant distribution is given by $\Gamma_{I+}(s) = e^{-(s-l)^2} + e^{-(s+l)^2}$ for some $l > 0$ and $\Gamma_{I-}(s) = 0$, which for $l \gtrsim 0.71$ has two maxima at $\pm s_m$ with $s_m > 0$ and so we expect pinching to occur at two points $s_r = \pm s_m$ (see § 4.6.1), with the consequence being that ‘satellite drops’ are formed. The parameter l is thus a geometric variable that controls how far apart the maxima are located. Upon replacing the definition of $K(s)$ with $K(s) := \frac{1}{4}(e^{-(s-l)^2} + e^{-(s+l)^2})$, expressions for h, H, \bar{u}, \bar{w} , and Γ_{\pm} are still given, respectively, by (4.17), (4.18), (4.19), (4.20) and (4.21a,b) along with conversion into Eulerian coordinates via (4.22). In order to discuss a real drop, one should consider the axisymmetric case rather than the two-dimensional set-up that is considered in this paper. As mentioned in the introduction, the formation of satellite drops due to rupture via Marangoni effects is an interesting avenue of research.

An example with parameters $C = 0.5$ and $l = 2$ is shown in figure 5. In particular, figure 5(a) shows the initial surfactant concentration $\Gamma_{I+}(s) = e^{-(s-2)^2} + e^{-(s+2)^2}$. From (4.17), we have that the point of minimum thickness (pinch off) rupture occurs near $s_m \approx \pm 2$. For example, figure 5(b) shows the sheet profile $H \pm \frac{1}{2}h$ (black curves) at $t = 10$, with a satellite drop around $x = 0$.

A point of physical interest in areas such as aerosol production at the ocean–air interface is the volume of the satellite droplet that is formed. In our framework, the volume (since we have a two-dimensional set-up, really, a surface area) of the droplet produced, V , can

Asymmetric Marangoni flow

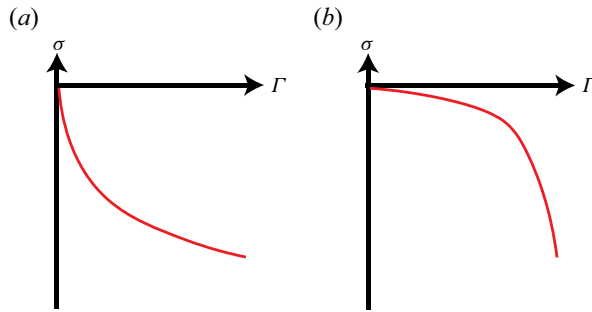


Figure 6. Schematic diagram of an isotherm $\sigma = \sigma(\Gamma)$ that is (a) convex or (b) concave. In general, we consider $\sigma = \sigma(\Gamma)$ strictly monotonically decreasing.

be written as

$$V = \int_{x(-s_m, t_r)}^{x(s_m, t_r)} h(x, t_r) dx \quad x = \int_{-s_m}^{s_m} ds = 2s_m. \quad (4.23)$$

For $l \gg 1$, $s_m \approx l$ and then $V \approx 2l$ and the volume of the satellite drop produced is just given by the spacing between the maxima (in fact, l does not need to be much greater than 1, e.g. $l = 1.4$ already gives $s_m = 1.399$ to 3 decimal places). In general, the same argument gives that if pinching occurs at two locations with Lagrangian coordinates $s_L < s_R$, then the volume of satellite drop produced is $V = s_R - s_L$.

4.6. Comparison between symmetry and asymmetry

In this section, we investigate the differences and similarities of a top–bottom asymmetric configuration and a top–bottom symmetric configuration for general surface tension isotherms $\sigma = \sigma(\Gamma)$. More explicitly, we compare the thinning and rupture of two cases given by the purely asymmetric case (PA),

$$\Gamma_{I+}^{PA}(s) = f(s) \quad \text{and} \quad \Gamma_{I-}^{PA}(s) = 0, \quad (4.24a,b)$$

and the ‘corresponding’ symmetric case (S),

$$\Gamma_{I+}^S(s) = \frac{1}{2}f(s) \quad \text{and} \quad \Gamma_{I-}^S(s) = \frac{1}{2}f(s). \quad (4.25a,b)$$

A function $F(x)$ is said to be *strictly monotonically decreasing* if $a > b \Rightarrow F(a) < F(b)$. In this section, we only consider surfactant isotherms $\sigma = \sigma(\Gamma)$ that are strictly monotonically decreasing. In other words, the addition of any amount of surfactant strictly decreases the surface tension. In § 4.6.1, we show that the rupture occurs at the Lagrangian point where f is maximal for both the purely asymmetric case (PA) and the symmetric case (S). In § 4.6.2, we show that the purely asymmetric case (PA) thins slower/faster than the symmetric case (S) when $\sigma = \sigma(\Gamma)$ is convex/concave (see figure 6). For comments about cases where there are surfactants on each side but not necessarily deposited symmetrically, see Appendix E, where it is found that the conclusions about the rate of thinning and convexity/concavity still hold. Experimentally, convexity and concavity can be observed for various surface tension isotherms (Prosser & Franses 2001; Liu & Duncan 2003; Erinin *et al.* 2023).

4.6.1. *Location of minimum thickness*

Here, we analyse the location of minimum thickness of the sheet h at a given time. In particular, this will give the location at which there is pinching. From (4.13), we have

$$\left. \frac{Dh^{PA}}{Dt} \right|_{(s,t)} = \frac{1}{4} \sigma(f(s)h^{PA}(s, t)) \tag{4.26}$$

and

$$\left. \frac{Dh^S}{Dt} \right|_{(s,t)} = \frac{1}{2} \sigma\left(\frac{1}{2}f(s)h^S(s, t)\right). \tag{4.27}$$

We first analyse the purely asymmetric case (PA). Consider two Lagrangian points denoted by s_1 and s_2 with $f(s_1) > f(s_2)$. Suppose that at some $t = t_e$, the thickness is equal at the two Lagrangian points $h^{PA}(s_1, t_e) = h^{PA}(s_2, t_e)$. Then, it follows from (4.26) that

$$\begin{aligned} \left. \frac{D}{Dt} \left(h^{PA}(s_1, t) - h^{PA}(s_2, t) \right) \right|_{t=t_e} &= \frac{1}{4} \left(\sigma\left(f(s_1)h^{PA}(s_1, t_e)\right) - \sigma\left(f(s_2)h^{PA}(s_2, t_e)\right) \right) \\ &< 0, \end{aligned} \tag{4.28}$$

where the inequality follows since σ is strictly monotonically decreasing and $f(s_1) > f(s_2)$. At $t = 0$, we have $h(s, t) = 1$ for all s . Thus, for $f(s_1) > f(s_2)$, we have

$$h^{PA}(s_1, t) < h^{PA}(s_2, t), \quad \forall t > 0 \tag{4.29}$$

and an analogous argument using (4.27) gives that

$$h^S(s_1, t) < h^S(s_2, t), \quad \forall t > 0. \tag{4.30}$$

Then, we deduce that the location of minimum thickness for both h^{PA} and h^S at any time $t > 0$ is given by the Lagrangian point s_m with maximum value for f (explicitly, $s_m := \arg \max_{s_0} f(s_0)$). In particular, the point of minimum thickness for the purely asymmetric case (PA) and symmetric case (S) will both be at the Lagrangian point $s_0 = s_m$. It should be noted that although the rupture point of the purely asymmetric case (PA) and symmetric case (S) is the same in Lagrangian coordinates, they need not be the same in Eulerian coordinates.

4.6.2. *Rate of thinning*

Another natural question to ask would be whether the purely asymmetric case (PA) thins faster/slower and, hence, pinches off earlier/later than the symmetric case (S). In order to analyse this problem, we consider two cases where (i) $\sigma = \sigma(\Gamma)$ is convex and (ii) $\sigma = \sigma(\Gamma)$ is concave (see figure 6). From (4.26) and (4.27), we have

$$\left. \frac{D(h^{PA} - h^S)}{Dt} \right|_{(s,t)} = \frac{1}{4} \left(\sigma(f(s)h^{PA}(s, t)) - 2\sigma\left(\frac{1}{2}f(s)h^S(s, t)\right) \right), \tag{4.31}$$

which we now analyse. From the definition of convexity and concavity, if $\sigma = \sigma(\Gamma)$ is convex, then for $a \in \mathbb{R}$,

$$\frac{\sigma(a) + \sigma(0)}{2} \geq \sigma\left(\frac{1}{2}a\right) \tag{4.32}$$

Asymmetric Marangoni flow

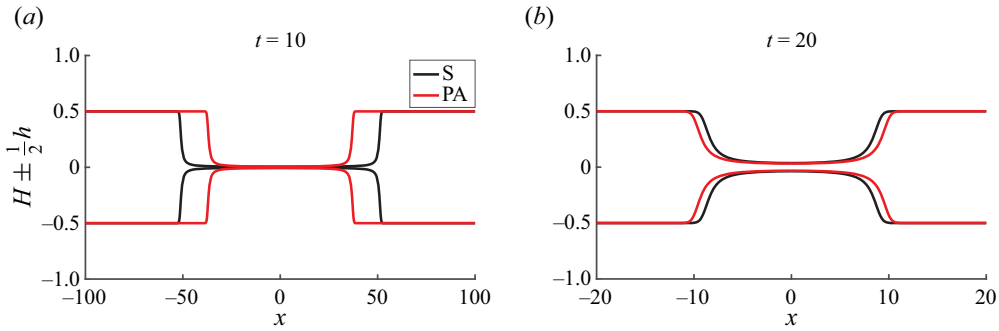


Figure 7. The symmetric case (S) (black curves) and the purely asymmetric case (PA) (red curves) are plotted for (a) $\sigma(\Gamma) = \Gamma(\Gamma - 2)$ at $t = 10$ and (b) $\sigma(\Gamma) = \log(1 - \Gamma/2)$ at $t = 20$. The curves plotted are the sheet profile $H \pm \frac{1}{2}h$. The spatial variable x is in Eulerian coordinates. In both cases, the initial surfactant concentration is given by $\Gamma_{I+}(x) = e^{-x^2}$ and $\Gamma_{I-}(x) = 0$. $C = 0.5$. For the non-dimensionalisation, see (4.1).

and if $\sigma = \sigma(\Gamma)$ is concave, then

$$\frac{\sigma(a) + \sigma(0)}{2} \leq \sigma\left(\frac{1}{2}a\right). \quad (4.33)$$

Furthermore, since $\sigma(\Gamma)$ is monotonically decreasing and $\sigma(0) = 0$, we have that if $\sigma = \sigma(\Gamma)$ is convex and $h^{PA}(s, t) \geq h^S(s, t)$, then

$$\sigma(f(s)h^{PA}(s, t)) \geq 2\sigma\left(\frac{1}{2}f(s)h^{PA}(s, t)\right) \geq 2\sigma\left(\frac{1}{2}f(s)h^S(s, t)\right) \quad (4.34)$$

and if $\sigma = \sigma(\Gamma)$ is concave and $h^{PA}(s, t) \leq h^S(s, t)$, then

$$\sigma(f(s)h^{PA}(s, t)) \leq 2\sigma\left(\frac{1}{2}f(s)h^{PA}(s, t)\right) \leq 2\sigma\left(\frac{1}{2}f(s)h^S(s, t)\right). \quad (4.35)$$

At that initial time, $h^{PA}(s, 0) = h^S(s, 0) = 1$. Thus, from (4.31), (4.34) and (4.35), we deduce that

$$h^{PA}(s, t) \geq h^S(s, t) \quad \forall t \text{ if } \sigma = \sigma(\Gamma) \text{ is convex} \quad (4.36)$$

and

$$h^{PA}(s, t) \leq h^S(s, t) \quad \forall t \text{ if } \sigma = \sigma(\Gamma) \text{ is concave,} \quad (4.37)$$

which, in other words, says that the purely asymmetric case (PA) thins slower/faster than the symmetric case (S) if $\sigma = \sigma(\Gamma)$ is convex/concave. The conclusion also holds when considering a general asymmetric case (see Appendix E). The conclusion makes sense physically, because a convex/concave $\sigma = \sigma(\Gamma)$ means that the decrease of surface tension is smaller/greater with a larger concentration of surfactant. The purely asymmetric case (PA) would correspondingly have smaller/larger total Marangoni stress than the symmetric case (S).

In figure 7, for $C = 0.5$, we compare the symmetric case (S) (black curves) and the purely asymmetric case (PA) (red curves) with results reported for (a) $\sigma(\Gamma) = \Gamma(\Gamma - 2)$ for $\Gamma \in [0, 1]$ at $t = 10$ and (b) $\sigma(\Gamma) = \log(1 - \Gamma/2)$ at $t = 20$. In both cases, the initial surfactant concentration is given by $\Gamma_{I+}(x) = e^{-x^2}$ and $\Gamma_{I-}(x) = 0$. The curves plotted are the sheet profile $H \pm \frac{1}{2}h$. The isotherm $\sigma = \Gamma(\Gamma - 2)$ is chosen to represent some

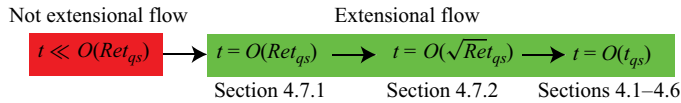


Figure 8. Summary of timescales in § 4. For $t \ll O(Re t_{qs})$, the flow is not extensional (red) (see Appendix B). For $t = O(Re t_{qs})$ or greater, the flow is extensional (green) (see Appendix B). Three timescales are discussed in § 4: $t = O(Re t_{qs})$ (§ 4.7.1), $t = O(\sqrt{Re} t_{qs})$ (§ 4.7.2) and $t = O(t_{qs})$ (§§ 4.1–4.6).

convex isotherm (strictly monotonically decreasing for $\Gamma \in [0, 1]$). The isotherm $\sigma(\Gamma) = \log(1 - \Gamma/2)$ is chosen to represent an example of a concave isotherm with motivation from the Langmuir isotherm. As expected from (4.36), we see that in figure 7(a) the symmetric case pinches faster than the purely asymmetric case. Similarly, as expected from (4.37), we see in figure 7(b) that the symmetric case pinches more slowly than the asymmetric case. A small point to note is that figure 7 is given in Eulerian coordinates (whereas (4.36) and (4.37) are results in Lagrangian coordinates).

4.7. Early time behaviour

In this subsection, we discuss the early time behaviour for the initial conditions (4.5) and boundary conditions (4.6). It is common in low-Reynolds-number flow analyses to consider inertia at early times in order to analyse how the quasi-static (inertialess) balance is obtained. For the case of liquid sheets and threads, see Buckmaster, Nachman & Ting (1975) and Howell (1996). For many problems, the exact details of the shorter timescale is not as interesting as the later time thinning and pinching as described in §§ 4.1–4.6. Thus, we keep discussions in this section brief. In particular, we only consider $\epsilon^2 \ll Re \ll 1$. For even smaller Re , analogous approaches can be considered, but the exact equations are different (see Howell 1996). In this subsection, we work in Eulerian coordinates.

The main timescale (dimensional) for thinning as described in prior sections is $t_{qs} = \epsilon \mu \mathcal{L} / \Delta \Sigma$. There are two shorter timescales. The first is the timescale (dimensional) $Re t_{qs}$, which evolves the horizontal velocity \bar{u} , and the second is the timescale (dimensional) $\sqrt{Re} t_{qs}$, which evolves the centreline H . Note that since $Re \ll 1$, we have separation of three timescales $Re t_{qs} \ll \sqrt{Re} t_{qs} \ll t_{qs}$, which is a familiar concept in asymptotics (Hinch 1991). It will be shown in §§ 4.7.1 and 4.7.2 that on the timescale $Re t_{qs}$, the horizontal velocity \bar{u} evolves as a diffusion equation and on the timescale $\sqrt{Re} t_{qs}$ the centreline H evolves as a wave equation. For a summary of the timescales, see figure 8. The evolution of \bar{u} on the timescale $Re t_{qs}$ is an inner solution for the centreline evolution H on the timescale $\sqrt{Re} t_{qs}$, which, in turn, is an inner solution for the quasi-static evolution as considered in §§ 4.1–4.6.

4.7.1. Diffusion equation for horizontal velocity \bar{u}

On the dimensional timescale $Re t_{qs}$, the non-dimensionalisation is now given by

$$\left. \begin{aligned} x = \mathcal{L}\tilde{x}, \quad u = \frac{\Delta \Sigma}{\epsilon \mu} \tilde{u}, \quad H = \epsilon \mathcal{L} \tilde{H}, \quad t = Re \frac{\epsilon \mu \mathcal{L}}{\Delta \Sigma} \tilde{T}_1, \quad y = \epsilon \mathcal{L} \tilde{y}, \quad w = \frac{1}{Re} \frac{\Delta \Sigma}{\mu} \tilde{W}_1, \\ h = \epsilon \mathcal{L} \tilde{h}, \quad p = \frac{\Delta \Sigma}{\epsilon \mathcal{L}} \tilde{p}, \quad \sigma = \Sigma + \Delta \Sigma \tilde{\sigma}, \end{aligned} \right\} \quad (4.38)$$

and we may apply the same expansion techniques as shown in § 3. Then (again dropping the tildes), the analogues to (3.25), (3.26), (3.27), (3.28) and (4.4) are given, respectively,

by

$$\frac{\partial h}{\partial T_1} = 0, \tag{4.39}$$

$$\frac{\partial H}{\partial T_1} = \bar{W}_1, \tag{4.40}$$

$$h \frac{\partial \bar{u}}{\partial T_1} = \left(\frac{\partial \sigma_+}{\partial x} + \frac{\partial \sigma_-}{\partial x} \right) + 4 \frac{\partial}{\partial x} \left(h \frac{\partial \bar{u}}{\partial x} \right), \tag{4.41}$$

$$h \frac{\partial \bar{W}_1}{\partial T_1} = 0, \tag{4.42}$$

$$\frac{\partial \Gamma_{\pm}}{\partial T_1} = 0. \tag{4.43}$$

We can immediately deduce from the initial conditions (4.5) that

$$h = 1, H = 0, \bar{W}_1 = 0, \Gamma_{\pm} = \Gamma_{I\pm}, \tag{4.44}$$

which then gives that

$$\frac{\partial \bar{u}}{\partial T_1} - 4 \frac{\partial^2 \bar{u}}{\partial x^2} = \frac{\partial}{\partial x} (\sigma(\Gamma_{I+}) + \sigma(\Gamma_{I-})). \tag{4.45}$$

Thus, we see that the evolution equation for \bar{u} is a diffusion equation with diffusion coefficient 4 and forcing given by the right-hand side of (4.45). From standard considerations of the diffusion equation (see [Appendix F](#)), it can then be deduced that

$$\lim_{T_1 \rightarrow \infty} \frac{\partial \bar{u}}{\partial x} = -\frac{1}{4} (\sigma(\Gamma_{I+}) + \sigma(\Gamma_{I-})), \tag{4.46}$$

which satisfies the quasi-static balance (4.2) as expected. A subtle point to be made here is that the initial condition (4.5) is compatible with the boundary condition (4.6) because the early time dynamics discussed here respects the far-field condition $\partial \bar{u} / \partial x = 0$ (explicitly, $\lim_{x \rightarrow \pm \infty} \lim_{T_1 \rightarrow \infty} (\partial \bar{u} / \partial x) = 0$).

4.7.2. Wave equation for centreline H

On the dimensional timescale $\sqrt{Re} t_{qs}$, the non-dimensionalisation is now given by

$$\left. \begin{aligned} x = \mathcal{L}\tilde{x}, \quad u = \frac{\Delta \Sigma}{\epsilon \mu} \tilde{u}, \quad H = \epsilon \mathcal{L}\tilde{H}, \quad t = \sqrt{Re} \frac{\epsilon \mu \mathcal{L}}{\Delta \Sigma} \tilde{T}_2, \quad y = \epsilon \mathcal{L}\tilde{y}, \\ w = \frac{1}{\sqrt{Re}} \frac{\Delta \Sigma}{\mu} \tilde{W}_2, \quad h = \epsilon \mathcal{L}\tilde{h}, \quad p = \frac{\Delta \Sigma}{\epsilon \mathcal{L}} \tilde{p}, \quad \sigma = \Sigma + \Delta \Sigma \tilde{\sigma}, \end{aligned} \right\} \tag{4.47}$$

and we may apply the same expansion techniques as shown in § 3. Then, the analogues to (3.25), (3.26), (3.27), (3.28) and (4.4) are given, respectively, by

$$\frac{\partial h}{\partial T_2} = 0, \tag{4.48}$$

$$\frac{\partial H}{\partial T_2} = \bar{W}_2, \tag{4.49}$$

$$0 = \left(\frac{\partial \sigma_+}{\partial x} + \frac{\partial \sigma_-}{\partial x} \right) + 4 \frac{\partial}{\partial x} \left(h \frac{\partial \bar{u}}{\partial x} \right), \tag{4.50}$$

$$\begin{aligned} \frac{\partial \bar{W}_2}{\partial T_2} = & \frac{1}{2} \frac{\partial^2}{\partial x^2} (h(\sigma_+ - \sigma_-)) + \frac{\partial}{\partial x} \left(\frac{\partial H}{\partial x} \left(\frac{2}{C} + (\sigma_+ + \sigma_-) \right) \right) \\ & + 4 \frac{\partial}{\partial x} \left(h \frac{\partial H}{\partial x} \frac{\partial \bar{u}}{\partial x} \right), \end{aligned} \tag{4.51}$$

$$\frac{\partial \Gamma_{\pm}}{\partial T_2} = 0. \tag{4.52}$$

Regarding the shorter timescale T_1 (in dimensional variables, Ret_{qs}) of the evolution for \bar{u} described in § 4.7.1 as the inner solution, we deduce from (4.46) that on the timescale T_2 of centreline evolution,

$$\frac{\partial \bar{u}}{\partial x} = -\frac{1}{4} (\sigma(\Gamma_{I+}) + \sigma(\Gamma_{I-})), \tag{4.53}$$

along with

$$h = 1 \quad \text{and} \quad \Gamma_{\pm} = \Gamma_{I\pm}, \tag{4.54}$$

which can be substituted into (4.49) and (4.51) to get

$$\frac{\partial^2 H}{\partial T_2^2} - \frac{2}{C} \frac{\partial^2 H}{\partial x^2} = \frac{1}{2} \frac{\partial^2}{\partial x^2} (\sigma(\Gamma_{I+}) - \sigma(\Gamma_{I-})). \tag{4.55}$$

Equation (4.55) is a wave equation with wavespeed $c = \sqrt{2/C}$ and forcing term independent of T_2 given by the right-hand side of (4.55). In dimensional variables, the wavespeed is $(\Delta \Sigma / \epsilon \mu) Re^{-1/2} \sqrt{2/C}$. Thus, the solution can be written as

$$H = -\frac{1}{4c^2} (2g(x) - g(x - cT_2) - g(x + cT_2)), \tag{4.56}$$

where $g(x) := \sigma(\Gamma_{I+}(x)) - \sigma(\Gamma_{I-}(x))$. Equation (4.56) is the famous d’Alembert’s solution for the wave equation and can be interpreted as having two travelling waves, one travelling to the left with wavespeed c and one travelling to the right with wavespeed c . In particular, we may deduce that

$$\lim_{T_2 \rightarrow \infty} H = -\frac{C}{4} (\sigma(\Gamma_{I+}) - \sigma(\Gamma_{I-})), \tag{4.57}$$

which satisfies the quasi-static balance (4.3) as expected. Again, it should be noted that the initial condition (4.5) is, thus, compatible with the boundary condition (4.6) since the early time dynamics discussed here respects the far field condition $H = 0$.

5. Asymmetric deposition of insoluble surfactants onto a uniformly thinning sheet

In this section, we consider the localised deposition of insoluble surfactants onto the top, $z = H + \frac{1}{2}h$, of a uniformly extending sheet of initial uniform thickness $h = h_I$ (the bottom, $z = H - \frac{1}{2}h$, remains clean) with initial horizontal velocity $u = \alpha x$ for α constant. Without surfactants, we assume that $\sigma_{\pm} = \Sigma = \text{constant}$. We assume that the Péclet number, defined by $\mathcal{L}^2\alpha/D$ is large enough such that diffusion may be ignored. We consider $Re \ll 1$. For the configuration considered in this section, there is a non-zero extensional flow at the initial time. Thus, unlike for the configuration considered in § 4, where the sheet is otherwise at rest (see Appendix B), the flow is extensional at all times.

Much of the analysis is similar to the example considered in § 4 and details are therefore omitted. In particular, we omit the discussion of the evolution starting with an initial surfactant concentration with a double maximum, which leads to satellite drops, since this is equivalent to § 4.5.

Similarly, we omit the discussion of the effect of convexity/concavity of surface tension isotherms, which would be equivalent to § 4.6. The two conclusions still hold, that is: (a) the location of minimum thickness for h^{PA} and h^S is given by $s_m := \arg \max_{s_0} f(s_0)$ and (b) h^{PA} thins faster/slower than h^S if $\sigma = \sigma(\Gamma)$ is convex/concave.

The choice of the initial condition $h = h_I$ and $u = \alpha x$ is physically and mathematically motivated. Large bare viscous surface bubbles have films that thin exponentially with respect to time (Debrégeas *et al.* 1998). The evolution of a uniform sheet with constant extension rate is, by definition, given by $h = h_I e^{-\alpha t}$ and $u = \alpha x$. Thus, the initial condition corresponds mathematically to a sheet that would otherwise be exponentially thinning uniformly. This initial condition is also the simplest case of extensional flow with nonzero velocity gradient $\partial u/\partial x$. In addition, the profile of a uniformly thinning sheet with constant extension, $h = h_I e^{-\alpha t}$ and $u = \alpha x$, is considered when discussing the thin-film region in foams (Breward & Howell 2002). However, for a large bare viscous surface bubble, Bartlett *et al.* (2023) has recently shown that the thickness is, in fact, not uniform.

We compare the physical relevance of the example in this section to the surface bubble drainage experiment given by Debrégeas *et al.* (1998). Consider physical values when a viscous surface bubble of radius ≈ 6 mm starts to exponentially thin (e.g. $t \approx 200$ s in figure 1 of Debrégeas *et al.* 1998). Here, the characteristic thickness ≈ 20 μm , horizontal length $\mathcal{L} \approx 6$ mm, viscosity $\mu \approx 10^3$ Pa s, density $\rho \approx 10^3$ kg m⁻³, surface tension $\Sigma \approx 2 \times 10^{-2}$ N m⁻¹ and inverse timescale $\alpha \approx 10^{-2}$ s⁻¹. Then, $\epsilon \approx 3 \times 10^{-3}$ and upon identifying $\mathcal{U} = \mathcal{L}\alpha$, we have $Re = \rho\mathcal{L}^2\alpha/\mu \approx 4 \times 10^{-7}$ and $C = \epsilon\mu\mathcal{L}\alpha/\Sigma \approx 0.01$. As shown in § 3.2, we require $Re = O(1)$ or less and $C = O(1)$ or greater in order for the extensional flow approximation to be valid, along with $M = O(1)$ or less.

The flow field $h = h_I e^{-\alpha t}$ and $u = \alpha x$ satisfies conservation of mass (3.25) but only satisfies conservation of horizontal momentum (3.27) in the case where inertia can be ignored to leading order, since $Re\bar{u}(\partial\bar{u}/\partial x)$ is not zero. Thus, it only makes sense to discuss the example when $Re \ll 1$. However, once again, inertia is important at early times.

5.1. Non-dimensional equations

Non-dimensionalise the equations according to (3.1) with $\mathcal{U} = \mathcal{L}\alpha$ (in other words, consider the timescale of the background exponentially thinning flow), where $\epsilon = h_I/\mathcal{L}$.

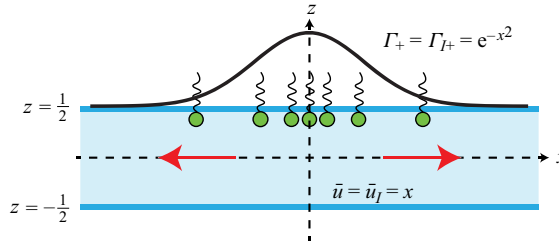


Figure 9. Initial set-up considered in § 5.4. An initial Gaussian surfactant distribution $\Gamma_{I+}(x) = e^{-x^2}$, $\Gamma_{I-}(x) = 0$ is deposited on top of a uniform sheet $-\frac{1}{2} \leq z \leq \frac{1}{2}$ at $t = 0$ with initial condition for horizontal velocity given by $\tilde{u}_I(x) = x$. The horizontal direction is given by the x axis and the vertical direction is given by the z axis. The red arrows denote the direction of horizontal flow. See (5.1) for the non-dimensionalisation.

In addition, non-dimensionalise the surfactant concentration with a characteristic surfactant concentration Γ_c . Explicitly,

$$\left. \begin{aligned} x &= \mathcal{L}\tilde{x}, & u &= \mathcal{L}\alpha\tilde{u}, & H &= \epsilon\mathcal{L}\tilde{H}, & t &= \frac{1}{\tilde{t}}, & y &= \mathcal{L}\tilde{y}, & w &= \epsilon\alpha\mathcal{L}\tilde{w}, \\ h &= \epsilon\mathcal{L}\tilde{h}, & \sigma &= \Sigma + \Delta\Sigma\frac{\alpha}{\tilde{\sigma}}, & \Gamma &= \Gamma_c\tilde{\Gamma}, \end{aligned} \right\} \quad (5.1)$$

We then have parameters $M = \Delta\Sigma/\epsilon\mu\mathcal{L}\alpha$, $Re = \rho\mathcal{L}^2\alpha/\mu$ and $C = \epsilon\mu\mathcal{L}\alpha/\Sigma$. Again, the tilde ($\tilde{}$) is dropped. We consider $M = O(1)$ or less and $C = O(1)$ or more so that we have extensional flow (see § 3.2). The horizontal length scale \mathcal{L} is once again given by the width of variation of the initial surfactant concentration.

Equations for h and H are given by (3.25) and (3.26). The equations for \tilde{u} and \tilde{w} are given by (3.27) and (3.28) with the inertia term neglected (note that unlike § 4, the constant M is not necessarily 1). Diffusion is ignored once again by assuming a large enough Péclet number $\mathcal{L}^2\alpha/D$ (diffusion coefficient D). Thus, Γ is given by (4.4).

5.2. Initial and boundary conditions

For the initial conditions, we consider a uniform sheet with constant extension, along with some initial surfactant distribution $\Gamma_{I\pm}(x)$ where $\Gamma_{\pm} \rightarrow 0$ as $x \rightarrow \pm\infty$. Far-field conditions are taken for the boundary condition. See figure 9 for a particular example where $\Gamma_{I+} = e^{-x^2}$ and $\Gamma_{I-} = 0$, which is considered in § 5.4. Explicitly,

$$h = 1, \quad H = 0, \quad \tilde{u} = x, \quad \tilde{w} = 0, \quad \Gamma_{\pm} = \Gamma_{I\pm} \quad \text{at } t = 0 \quad (5.2)$$

and

$$h = e^{-t}, \quad H = 0, \quad \frac{\partial \tilde{u}}{\partial x} = 1, \quad \tilde{w} = 0, \quad \Gamma_{\pm} = 0 \quad \text{at } x = \pm\infty, \quad (5.3)$$

where it should be noted here that $x = \pm\infty$ more rigorously means some $1 \ll x \ll Re^{-1}$ (in order for the inertia terms to be neglected, $Re\tilde{u}(\partial\tilde{u}/\partial x) = Rex \ll 1$).

Asymmetric Marangoni flow

5.3. *Lagrangian coordinates*

We may proceed with the same technique as in § 4.3 to deduce the equivalent equations to (4.7), (4.8), (4.12), (4.13), (4.14) and (4.15):

$$\frac{\partial \bar{u}}{\partial x} = -\frac{M}{4h(x, t)} (\sigma(\Gamma_+(x, t)) + \sigma(\Gamma_-(x, t))) + \frac{e^{-t}}{h(x, t)}, \quad (5.4)$$

$$H(x, t) = -\frac{M}{2} \frac{h(\sigma(\Gamma_+(x, t)) - \sigma(\Gamma_-(x, t)))}{\left(\frac{2}{C} + 4e^{-t}\right)}, \quad (5.5)$$

$$\Gamma_{\pm}(s, t) = \Gamma_{I\pm}(s)h(s, t), \quad (5.6)$$

$$\left. \frac{Dh}{Dt} \right|_{(s,t)} = \frac{M}{4} (\sigma(\Gamma_{I+}(s)h(s, t)) + \sigma(\Gamma_{I-}(s)h(s, t))) - e^{-t}, \quad (5.7)$$

$$\bar{w}(s, t) = \left. \frac{DH}{Dt} \right|_{(s,t)}, \quad (5.8)$$

$$\left. \frac{\partial x}{\partial s} \right|_{(s,t)} = \frac{1}{h(s, t)}. \quad (5.9)$$

5.4. *Example: linear isotherm, Gaussian deposition on top*

In this subsection, we consider the example where the initial surfactant distribution given by $\Gamma_{I+}(s) = e^{-s^2}$ and $\Gamma_{I-}(s) = 0$ and the surface tension isotherm is linear $\sigma(\Gamma) = -\Gamma$ (see figure 9 for the set-up). Then, we have

$$\left. \frac{Dh}{Dt} \right|_{(s,t)} = -K(s)h(s, t) - e^{-t}, \quad (5.10)$$

where $K(s) := (M/4)e^{-s^2}$. Using the initial condition $h(s, 0) = 1$, we have the analytic solution

$$h(s, t) = \begin{cases} \frac{e^{-t}}{1 - K(s)} - \frac{K(s)}{1 - K(s)} e^{-K(s)t}, & K(s) \neq 1, \\ (1 - t)e^{-t}, & K(s) = 1, \end{cases} \quad (5.11)$$

where we note that the point $K(s) = 1$ is not a discontinuity since

$$\lim_{k \rightarrow 1} \left(\frac{e^{-t}}{1 - k} - \frac{k}{1 - k} e^{-kt} \right) = (1 - t)e^{-t}. \quad (5.12)$$

Noting that $x(0, t) = 0$ by symmetry, we have from (5.9) that

$$x(s, t) = \int_0^s \frac{1}{h(s', t)} ds'. \quad (5.13)$$

The equations for H , \bar{u} , \bar{w} and Γ_{\pm} are given by

$$H(s, t) = \frac{2K(s)h(s, t)^2}{\left(\frac{2}{C} + 4e^{-t}\right)}, \tag{5.14}$$

$$\bar{u}(s, t) = \int_0^s \frac{K(s')}{h(s', t)} + \frac{e^{-t}}{h^2(s', t)} ds', \tag{5.15}$$

$$\bar{w}(s, t) = -\frac{4K(s)h(s, t)}{\left(\frac{2}{C} + 4e^{-t}\right)} (K(s)h(s, t) + e^{-t}) + \frac{8e^{-t}K(s)h(s, t)^2}{\left(\frac{2}{C} + 4e^{-t}\right)^2}, \tag{5.16}$$

$$\Gamma_+(s, t) = \frac{4}{M}K(s)h(s, t), \quad \Gamma_-(s, t) = 0. \tag{5.17}$$

5.4.1. *Description of the solution*

First, we note from (5.11) that $h(s, t) = 0$ when $t = (1/(K(s) - 1)) \log(K(s))$ for $K(s) \neq 1$ or when $t = 1$ for $K(s) = 1$. Thus, rupture occurs at time $t = t_r$ and location $s = s_r$ where

$$t_r = \min_s \begin{cases} \frac{1}{K(s) - 1} \log(K(s)), & K(s) \neq 1, \\ 1, & K(s) = 1, \end{cases} \tag{5.18}$$

and

$$s_r = \arg \min_s \begin{cases} \frac{1}{K(s) - 1} \log(K(s)), & K(s) \neq 1, \\ 1, & K(s) = 1, \end{cases} \tag{5.19}$$

which, by noting that the function $f(k) := \log(k)/(k - 1)$ is a strictly decreasing function of $x > 0$, can be evaluated as

$$t_r = \begin{cases} \frac{1}{\frac{M}{4} - 1} \log\left(\frac{M}{4}\right), & M \neq 4, \\ 1, & M = 4, \end{cases} \tag{5.20}$$

and

$$s_r = 0. \tag{5.21}$$

There is no discontinuity once again since $\lim_{M \rightarrow 4} (1/(M/4 - 1)) \log(M/4) = 1$.

It is interesting to note that for any $M > 0$, finite time rupture now occurs (in contrast to the case without surfactants where the sheet is exponentially thinning $h = e^{-t}$). The fact that $s_r = 0$ follows once again from the more general notion that rupture occurs at the Lagrangian point of maximum Γ .

Previously, we analysed where and when the sheet ruptures. We may also analyse how the sheet ruptures. Again, a point of caution is that this paper does not include van der

Asymmetric Marangoni flow

Waals forces. As shown in [Appendix G](#), we have for $s \ll 1$ and $0 < t^* := t_r - t \ll 1$ that

$$h(s, t^*) = c_1 t^* + c_2 s^2 \tag{5.22}$$

and

$$x(s, t^*) = \frac{1}{\sqrt{c_1 c_2 t^*}} \arctan \left(\frac{s}{\sqrt{\frac{c_1}{c_2} t^*}} \right), \tag{5.23}$$

where c_1, c_2 are explicit functions of M , given by [\(G2\)](#). Equations [\(5.22\)](#) and [\(5.23\)](#) can be rewritten as self-similar solutions

$$h(\eta, t^*) = c_1 t^* (1 + \eta^2) \tag{5.24}$$

and

$$x(\eta, t^*) = \frac{1}{\sqrt{c_1 c_2 t^*}} \arctan(\eta), \tag{5.25}$$

where $\eta := s((c_1/c_2)t^*)^{-1/2}$ is the self-similarity variable. Inverting [\(5.23\)](#) and substituting into [\(5.22\)](#) gives that near the pinch ($s \ll 1, t^* \ll 1$), h is given in Eulerian coordinates by

$$h(x, t^*) = c_1 t^* \left(1 + \tan^2 \left(x \sqrt{c_1 c_2 t^*} \right) \right). \tag{5.26}$$

An example with $M = 4$ and $C = 0.5$ (representative of parameter values with $M = O(1)$ and $C = O(1)$) is given in [figure 10](#). The value $M = 4$ has the nice property from [\(5.20\)](#) that the sheet ruptures at $t = 1$. [Figure 10\(a\)](#) shows the bottom of the sheet $H - \frac{1}{2}h$, the centreline H , the top of the sheet $H + \frac{1}{2}h$, and the surfactant distribution Γ_+ at the initial time. Again, by initial time, we mean $t = 0$ where a quasi-static balance has been achieved and so, in particular, the centreline is bent (see §§ [5.1](#) and [5.5](#)). [Figure 10\(b\)](#) shows the velocity profiles $\bar{u} - x$ and \bar{w} at the initial time. The value $\bar{u} - x$ is plotted rather than \bar{u} for better visualisation. Similarly, [figure 10\(c,d\)](#) report the variables at $t = 0.5$ and [figure 10\(e,f\)](#) report the variables at $t = 0.9$ (which is close to the rupture time $t_r = 1$). The times $t = 0.5$ and 0.9 were chosen to represent mid and late times, respectively, for the thinning problem.

The non-uniform surfactant distribution means that there are Marangoni effects, where surfactants spread from a region of high concentration to low concentration (see [figure 10\(a,c,e\)](#)), since low-concentration regions have higher surface tension. As result of the horizontal velocity \bar{u} induced by the spreading of surfactants, h decreases and the sheet thins, in addition to the background exponentially thinning given by e^{-t} ; see [figure 10\(a,c,e\)](#).

5.5. Early time behaviour

Again, we only consider $\epsilon^2 \ll Re \ll 1$. There are three timescales once again, given by $Re\alpha^{-1} \ll \sqrt{Re}\alpha^{-1} \ll \alpha^{-1}$. On the timescale $Re\alpha^{-1}$, the horizontal velocity \bar{u} evolves as

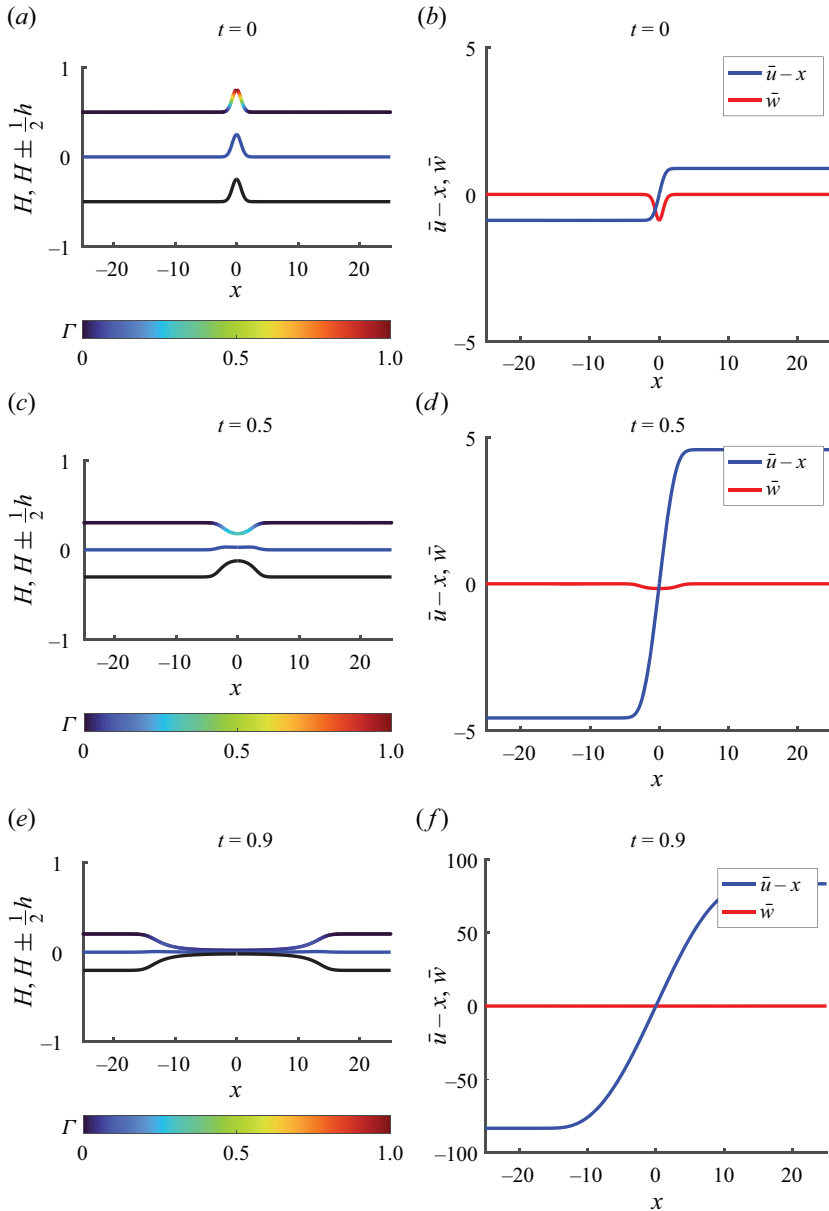


Figure 10. Time evolution with an imposed extensional flow. Plots of (5.11), (5.14), (5.15), (5.16), (5.17) and (5.13) for $M = 4$ and $C = 0.5$. The spatial variable x is in Eulerian coordinates. The three curves from bottom to top in (a) are $H - \frac{1}{2}h$ (black), H (blue), $H + \frac{1}{2}h$ (coloured with surfactant concentration Γ) at the initial time and (b) shows the velocity profiled $\bar{u} - x$ (blue) and \bar{w} (red) at the initial time. Similarly, (c,d) report the variables at $t = 0.5$ and (e,f) report the variables at $t = 0.9$. For the non-dimensionalisation, see (4.1).

a diffusion equation. Proceeding as in § 4.7.1, we deduce that

$$\frac{\partial \bar{u}}{\partial T_1} - 4 \frac{\partial^2 \bar{u}}{\partial x^2} = M \frac{\partial}{\partial x} (\sigma(\Gamma_{I+}) + \sigma(\Gamma_{I-})) \tag{5.27}$$

with the limit $T_1 \rightarrow \infty$ given by

$$\lim_{T_1 \rightarrow \infty} \frac{\partial \bar{u}}{\partial x} = 1 - \frac{M}{4} (\sigma(\Gamma_{I+}) + \sigma(\Gamma_{I-})). \quad (5.28)$$

On the timescale $\sqrt{Re}\alpha^{-1}$ the centreline H evolves as a wave equation. Proceeding as in § 4.7.2, we deduce that

$$\frac{\partial^2 H}{\partial T_2^2} - \left(4 + \frac{2}{C}\right) \frac{\partial^2 H}{\partial x^2} = \frac{M}{2} \frac{\partial^2}{\partial x^2} (\sigma(\Gamma_{I+}) - \sigma(\Gamma_{I-})), \quad (5.29)$$

which is the wave equation with wavespeed $c = \sqrt{(4 + 2/C)}$ and forcing term independent of T_2 given by the right-hand side of (5.29). In dimensional variables, the wavespeed is $\alpha \mathcal{L} Re^{-1/2} \sqrt{(4 + 2/C)}$. Thus, the solution can be written as

$$H = -\frac{M}{4c^2} (2g(x) - g(x - cT_2) - g(x + cT_2)), \quad (5.30)$$

where $g(x) := \sigma(\Gamma_{I+}(x)) - \sigma(\Gamma_{I-}(x))$. In particular, we may deduce that

$$\lim_{T_2 \rightarrow \infty} H = -\frac{M}{2 \left(4 + \frac{2}{C}\right)} (\sigma(\Gamma_{I+}) - \sigma(\Gamma_{I-})). \quad (5.31)$$

6. Discussion

In § 3, an asymptotic expansion was used to derive the leading-order thin-film equations in an extensional flow regime with Marangoni effects, where three conditions (3.9), (3.10) and (3.11) were identified to give extensional flow, i.e. $u \approx u(x, t)$, $p \approx p(x, t)$. In particular, the (3.26) and (3.28) allow for the inclusion of Marangoni effects into the evolution of the centreline H and the vertical velocity \bar{w} .

With the thin-film equations derived in § 4, the example of surfactant deposition on one side of a sheet (otherwise at rest) was considered. Then, in § 4.4, we presented an analysis of the film evolution following a Gaussian deposition of surfactant on top, for the case of a linear isotherm; a related example was treated in § 4.4. In particular, we considered three aspects of top–bottom asymmetry. The first was the centreline, given by a quasi-static solution (4.8) with early time evolution given by a wave equation as in § 4.7.2. Second, it was shown that the rupture location was the same in Lagrangian coordinates for both the purely asymmetric case (PA) and symmetric case (S). Then, the differences in thinning rates between the purely asymmetric case (PA) and symmetric case (S) were discussed with details depending on whether $\sigma = \sigma(\Gamma)$ was convex or concave. Finally, in § 5 we considered the surfactant deposition on one side of an otherwise uniformly thinning sheet. The analysis was similar to § 4. For a summary of the results, see table 1.

As part of our analyses, we considered the thinning and pinching of a liquid sheet due to Marangoni effects. A related experimental set-up, similar to that by Néel & Villermaux (2018), would be the deposition of insoluble surfactants on the top of a viscous planar film and subsequent measurement of the resulting centreline deformation. It would be interesting to see what happens after pinching has occurred, for example, by using ideas of ‘continuation’ that have been developed elsewhere (Eggers 2014; Eggers & Fontelos 2015). In addition, it may be beneficial to explore further the production of satellite drops from pinching due to Marangoni effects (see § 4.5), which, if relevant to a surface bubble,

	Stationary background (§ 4)	Uniformly thinning background (§ 5)
Sheet evolution (linear isotherm)	No finite time pinch off. (§ 4.4)	Finite time pinch off. (§ 5.4)
Satellite drop formation	Possible. (§ 4.5)	Possible.
Effects due to the shape of the surface tension isotherm	Convex \Rightarrow slower thinning. Concave \Rightarrow faster thinning. Thickness is at minimum at the Lagrangian point where $\Gamma_l(s)$ is maximal. (§ 4.6)	Convex \Rightarrow slower thinning. Concave \Rightarrow faster thinning. Thickness is at minimum at the Lagrangian point where $\Gamma_l(s)$ is maximal.
Early time evolution	\bar{u} evolves as a diffusion equation (4.45). H evolves as a wave equation (4.55).	\bar{u} evolves as a diffusion equation (5.27). H evolves as a wave equation (5.29).

Table 1. Summary of the results for the surfactant deposition problem.

would be an additional aerosol production mechanism in addition to the usual jet drops and film drops.

As mentioned in the introduction, asymmetric Marangoni flow configurations should occur in many physical systems, such as on the inside of a bubble and the outside of a bubble. In order to relate this study to naturally important setups such as air–water interfaces, it would be interesting to consider the case $Re \gg 1$.

Although the thin-film equations are commonly used in the literature to study thin-film Marangoni flows, a comparison to the full Navier–Stokes equations with Marangoni forces (see § 2) may be needed. We are currently considering the deposition of surfactants onto a liquid film using direct numerical simulation approaches for Marangoni flow with the numerical package developed by Farsoiya *et al.* (2024) in Basilisk (Popinet & Collaborators 2013).

Finally, it should be noted that the thinning and rupture of a liquid film is complex with many other different processes potentially involved such as evaporation (Poulain *et al.* 2018), salt concentration (Poulain *et al.* 2018; Dubitsky *et al.* 2023), marginal regeneration (Mysels, Shinoda & Frankel 1959; Lhuissier & Villermaux 2012; Gros *et al.* 2021; Miguet *et al.* 2021) and van der Waals forces (Erneux & Davis 1993). Consequently, it may be beneficial to also consider top–bottom asymmetry of liquid sheets for other physical mechanisms.

Supplementary material. Supplementary material is available at <https://doi.org/10.1017/jfm.2024.501>.

Acknowledgements. We thank P.K. Farsoiya for help with setting up the partial differential equations solver in Appendix C. We also thank the anonymous reviewers whose feedback helped to improve the manuscript.

Funding. This work was supported by NSF grant 1844932 to L.D., NSF grant 2127563 to H.A.S. and the Guggenheim Second Year Fellowship in the Department of Mechanical and Aerospace Engineering, Princeton University, to J.E.

Declaration of interests. The authors report no conflict of interest.

Author ORCIDs.

✉ Jun Eshima <https://orcid.org/0000-0003-3381-2999>;

✉ Luc Deike <https://orcid.org/0000-0002-4644-9909>;

✉ Howard A. Stone <https://orcid.org/0000-0002-9670-0639>.

Appendix A. Condition (3.11) for the case of symmetry

In the case of symmetry ($\sigma = \sigma_{\pm}, \kappa = \kappa_{\pm}$), the right-hand side of (3.11) can be replaced with the phrase ‘ $O(\epsilon^{-2})$ or less’. This can be explained when (3.19) is derived in § 3.3.

Consider the case $(\epsilon^2/C)(1 + MC\sigma_{\pm})\kappa_{\pm} = O(1)$. In addition, consider $M = O(1)$ or less; see (3.10). Then, $(\epsilon^2/C)(1 + MC\sigma_{\pm})\kappa_{\pm} \approx (\epsilon^2/C)\kappa_{\pm}$ to leading order in ϵ^2 and (3.19) becomes two equations,

$$\frac{\epsilon^2}{C}\kappa_{\pm} = p_0 + 2\frac{\partial u_0}{\partial x}, \tag{A1}$$

which implies that $\kappa_+ = \kappa_-$. Then, we must have $\kappa_+ = \kappa_-$ and consequently that $\partial^2 H/\partial x^2 = 0$ (Howell 1996), which gives a straight centreline, so there are no top–bottom asymmetries.

In the case that we have symmetry ($\sigma = \sigma_{\pm}, \kappa = \kappa_{\pm}$), the two equations become a single equation,

$$\frac{\epsilon^2}{C}\kappa = p_0 + 2\frac{\partial u_0}{\partial x}, \tag{A2}$$

and the rest of the derivation in § 3 can be followed while keeping the left-hand side of (A2). Then, the term $\frac{1}{2}(\epsilon^2/C)h(\partial^3 h/\partial x^3)$ appears on the right-hand side of (3.27), which is already familiar in the literature (De Wit *et al.* 1994). Thus, in the case of symmetry, the right-hand side of (3.11) can be replaced with the phrase ‘ $O(\epsilon^2)$ or less’. In other words, (3.11) is a condition that becomes more strict due to the asymmetry of interest.

Appendix B. Justification of extensional flow in § 4

Here, we give justification for only considering extensional flow in § 4. In this appendix, all variables are dimensional for clarity. Since the sheet starts at rest, there is a timescale t_a required for the horizontal velocity of the sheet to accelerate to the extensional flow scaling $\mathcal{U}_E := \Delta\Sigma/\epsilon\mu$. The scaling $\mathcal{U}_E = \Delta\Sigma/\epsilon\mu$ can be seen from balancing extensional stress with the Marangoni stress $(\mu(\partial/\partial x)(h(\partial u/\partial x)) \sim \partial\sigma_{\pm}/\partial x)$. We can give an estimate for the timescale (dimensional) t_a required for the horizontal velocity to reach $\mathcal{U}_E = \Delta\Sigma/\epsilon\mu$. From the horizontal force balance $(\rho h(\partial u/\partial t) \sim \partial\sigma_{\pm}/\partial x)$, we have

$$\rho\frac{\epsilon\mathcal{L}\mathcal{U}_E}{t_a} = \frac{\Delta\Sigma}{\mathcal{L}}, \tag{B1}$$

which rearranges to

$$t_a = \frac{\rho\mathcal{L}^2}{\mu}. \tag{B2}$$

As expected, the acceleration timescale t_a for the horizontal velocity is the same timescale as discussed in § 4.7.1, since $t_a = Re t_{qs}$ where $t_{qs} = \epsilon\mu\mathcal{L}/\Delta\Sigma$, $Re = \rho\mathcal{L}\Delta\Sigma/\epsilon\mu^2$. In conclusion, the flow is extensional for $t = O(t_a)$ or greater and not extensional for $t \ll O(t_a)$.

We now show that the details of the time $t \ll O(t_a)$, when the flow is not extensional, can be safely ignored for $Re = O(1)$ or less. Consider times $t \ll O(t_a)$. From the horizontal

force balance ($\rho h(\partial u/\partial t) \sim \partial \sigma_{\pm}/\partial x$),

$$\frac{|u|}{\mathcal{U}_E} \ll 1. \tag{B3}$$

From conservation of mass ($\partial h/\partial t \sim -h(\partial u/\partial x)$), we have that

$$\frac{|h - h_I|}{h_I} \sim \frac{t|u|}{\mathcal{L}} \ll \frac{t_a \mathcal{U}_E}{\mathcal{L}} = Re \tag{B4}$$

and similarly from continuity ($\partial w/\partial z \sim -(\partial u/\partial x)$), the kinematic condition ($\partial H/\partial t \sim w$) and conservation of surfactant ($\partial \Gamma_{\pm}/\partial t \sim -\Gamma_{\pm}(\partial u/\partial x)$), we deduce that (using $\epsilon = h_I/\mathcal{L}$)

$$\frac{|w|}{\epsilon \mathcal{U}_E} \ll 1 \quad \text{and} \quad \frac{|H|}{h_I}, \quad \frac{|\Gamma_{\pm} - \Gamma_{I\pm}|}{\Gamma_{I\pm}} \ll Re. \tag{B5}$$

Then, for $Re = O(1)$ or less, we have that

$$\frac{|h - h_I|}{h_I}, \quad \frac{|H|}{h_I}, \quad \frac{|u|}{\mathcal{U}_E}, \quad \frac{|w|}{\epsilon \mathcal{U}_E}, \quad \frac{|\Gamma_{\pm} - \Gamma_{I\pm}|}{\Gamma_{I\pm}} \ll 1. \tag{B6}$$

Thus, the values for h, H, u, w and Γ_{\pm} do not vary appreciably from the initial condition in the timescale $t \ll O(t_a)$ and the details of the timescale $t \ll O(t_a)$ can be safely ignored. In other words, we only need to consider the extensional flow regime for § 4.

Appendix C. The inclusion of inertia

We may compare the solutions of (3.27) and (3.28) with the inertialess solutions of (4.2) and (4.3). For the numerical solution, we use the one-dimensional PDE solver routine (src/grid/cartesian1D.h) on Basilisk (Popinet & Collaborators 2013). Note that for both cases, the evolution equations for h and H are given by (3.25) and (3.26). Solutions for (3.27) and (3.28) are obtained numerically subject to the initial conditions given by (4.5) and boundary conditions (4.6). The initial surfactant concentration is given by $\Gamma_{I+} = e^{-s^2}$ and $\Gamma_{I-} = 0$. We choose $C = 0.5$ and $M = 1$, which is the same set-up as in figure 4.

Figure 11(a) shows the sheet profile $H \pm \frac{1}{2}h$ at $t = 1$, where we compare the inertialess result (dashed black line), $Re = 10$ (solid blue line), $Re = 1$ (solid green line) and $Re = 0.001$ (solid red line). Figure 11(b) shows the same case as figure 11(a) but at $t = 10$ instead. The times $t = 1$ and $t = 10$ are chosen to represent mid and late times of the thinning problem (also chosen for figure 4). The horizontal direction x is Eulerian. As expected, the agreement between the inertialess solution (dashed black line) and the $Re = 0.001$ solution (solid red line) is good at both $t = 1$ and $t = 10$. As Re increases, we can see from figure 11(b) that the influence of inertia slows down the pinching at $x = 0$. The bumps on the sheet profile $H \pm \frac{1}{2}h$ for the $Re = 1$ curve (solid green line) at $x = \pm 20$ are the right and left travelling waves of the centreline deformation as described in § 4.7.2 (although it is not a direct comparison since § 4.7.2 considered $Re \ll 1$).

Appendix D. Derivation of the relationship between Eulerian and Lagrangian coordinates

Although the following approach is standard (Eggers & Fontelos 2015), the derivation of (4.15) is included below for completeness. Consider some fixed Lagrangian point s_f and a

Asymmetric Marangoni flow

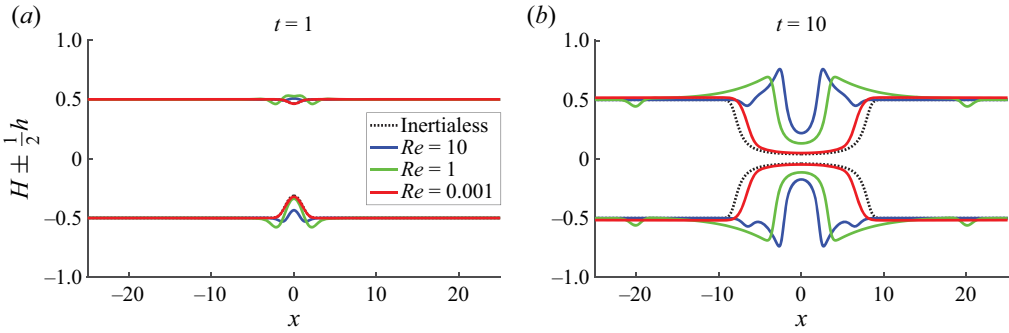


Figure 11. Effect of including inertia on the evolution of the liquid sheet. The curves are the solutions for the deposition problem with initial surfactant concentration given by $\Gamma_{I+}(s) = e^{-s^2}$ and $\Gamma_{I-}(s) = 0$ with parameters $C = 0.5$. (a) Sheet profile $H \pm \frac{1}{2}h$ at $t = 1$, where we compare the inertialess result (dashed black line), $Re = 10$, (solid blue line), $Re = 1$ (solid green line) and $Re = 0.001$ (solid red line). The horizontal direction x is Eulerian. (b) Same as (a) but at $t = 10$. The horizontal direction x is Eulerian.

variable Lagrangian point s . Then, by global conservation of mass

$$s - s_f = \int_{x(s_f, t)}^{x(s, t)} h(x', t) dx' = \int_{s_f}^s h(s', t) \frac{\partial x}{\partial s} \Big|_{(s', t)} ds', \quad (\text{D1})$$

which upon taking the derivative with respect to s gives

$$1 = h(s, t) \frac{\partial x}{\partial s} \Big|_{(s, t)} \quad (\text{D2})$$

as required.

Appendix E. General asymmetric setups

Consider the general asymmetric case (A), where there are surfactants on each side but not necessarily symmetrically deposited. Explicitly, the surfactant concentrations are given by

$$\Gamma_{I+}^A(s) = f(s), \quad \Gamma_{I-}^A(s) = g(s), \quad (\text{E1})$$

for some $f(s), g(s)$. The ‘corresponding’ symmetric case (S) is given by

$$\Gamma_{I\pm}^S(s) = \frac{1}{2} (f(s) + g(s)). \quad (\text{E2})$$

Then, we may proceed as in § 4.6.2, to deduce that

$$\begin{aligned} \frac{D(h^A - h^S)}{Dt} \Big|_{(s, t)} &= \frac{1}{4} \left(\sigma \left(f(s)h^A(s, t) \right) + \sigma \left(g(s)h^A(s, t) \right) \right. \\ &\quad \left. - 2\sigma \left(\frac{1}{2} (f(s) + g(s)) h^S(s, t) \right) \right), \end{aligned} \quad (\text{E3})$$

which we will now analyse. From the definition of convexity and concavity, if $\sigma = \sigma(\Gamma)$ is convex, then for $a, b \in \mathbb{R}$,

$$\frac{1}{2} (\sigma(a) + \sigma(b)) \geq \sigma \left(\frac{1}{2} (a + b) \right) \quad (\text{E4})$$

and if $\sigma = \sigma(\Gamma)$ is concave, then

$$\frac{1}{2} (\sigma(a) + \sigma(b)) \leq \sigma\left(\frac{1}{2}(a+b)\right). \tag{E5}$$

Furthermore, since $\sigma(\Gamma)$ is monotonically decreasing, we have that if $\sigma = \sigma(\Gamma)$ is convex and $h^A \geq h^S$, then

$$\begin{aligned} \sigma\left(f(s)h^A(s,t)\right) + \sigma\left(g(s)h^A(s,t)\right) &\geq 2\sigma\left(\frac{1}{2}(f(s)+g(s))h^A(s,t)\right) \\ &\geq 2\sigma\left(\frac{1}{2}(f(s)+g(s))h^S(s,t)\right) \end{aligned} \tag{E6}$$

and if $\sigma = \sigma(\Gamma)$ is concave and $h^A \leq h^S$, then

$$\begin{aligned} \sigma\left(f(s)h^A(s,t)\right) + \sigma\left(g(s)h^A(s,t)\right) &\leq 2\sigma\left(\frac{1}{2}(f(s)+g(s))h^A(s,t)\right) \\ &\leq 2\sigma\left(\frac{1}{2}(f(s)+g(s))h^S(s,t)\right). \end{aligned} \tag{E7}$$

At initial time, $h^A(s, 0) = h^S(s, 0) = 1$. Thus, from (E3), (E6), (E7), we deduce that

$$h^A(s, t) \geq h^S(s, t) \quad \forall t \text{ if } \sigma = \sigma(\Gamma) \text{ is convex} \tag{E8}$$

and

$$h^A(s, t) \leq h^S(s, t) \quad \forall t \text{ if } \sigma = \sigma(\Gamma) \text{ is concave.} \tag{E9}$$

The location of the rupture is more complicated. With the same argument as in § 4.6.1, we deduce that for the particular case where both $f(s_1) > f(s_2)$ and $g(s_1) > g(s_2)$, then

$$h^A(s_1, t) < h^A(s_2, t), \quad \forall t > 0. \tag{E10}$$

Appendix F. The limit $T_1 \rightarrow \infty$ of the diffusion equation

From (4.45), by letting $u = u' - F(x)$ with

$$F(x) := \int_0^x \frac{1}{4} (\sigma(\Gamma_{I^+}(y)) + \sigma(\Gamma_{I^-}(y))) dy, \tag{F1}$$

we have

$$\frac{\partial u'}{\partial T_1} - 4 \frac{\partial^2 u'}{\partial x^2} = 0 \tag{F2}$$

with initial condition $u'(x, 0) = F(x)$. Throughout this paper, we only consider examples where $F(-\infty)$ and $F(\infty)$ are finite. Then, as is usual for a diffusion equation, the solution

is given by

$$u'(x, T_1) = \frac{1}{\sqrt{16\pi T_1}} \int_{-\infty}^{\infty} F(y) \exp\left(\frac{-(x-y)^2}{16T_1}\right) dy, \tag{F3}$$

which upon a change of variables gives

$$u'(x, T_1) = \frac{1}{\sqrt{\pi}} \int_{-\infty}^{\infty} F(x + 4\sqrt{T_1}v) e^{-v^2} dv. \tag{F4}$$

Hence,

$$\lim_{T_1 \rightarrow \infty} u'(x, T_1) = \frac{1}{\sqrt{\pi}} \int_{-\infty}^{\infty} \lim_{T_1 \rightarrow \infty} F(x + 4\sqrt{T_1}v) e^{-v^2} dv = \frac{1}{2} (F(\infty) + F(-\infty)), \tag{F5}$$

where upon noting that F is bounded everywhere: $F(-\infty) \leq F(y) \leq F(\infty)$, the limit was passed under the integral sign using the dominated convergence theorem (Billingsley 2017). Thus, in total, we have

$$\lim_{T_1 \rightarrow \infty} u(x, T_1) = -F(x) + \frac{1}{2} (F(\infty) + F(-\infty)). \tag{F6}$$

In particular, we obtain (4.46):

$$\lim_{T_1 \rightarrow \infty} \frac{\partial \bar{u}}{\partial x} = -\frac{1}{4} (\sigma(\Gamma_{I+}) + \sigma(\Gamma_{I-})). \tag{F7}$$

Appendix G. Derivation of the shape of the pinch in § 5

Upon expanding (5.11) for $s \ll 1$ and $t^* \ll 1$, we have with errors at $O(s^4, s^2 t^*, (t^*)^2)$:

$$h(s, t^*) = c_1 t^* + c_2 s^2, \tag{G1}$$

where

$$c_1 = e^{-t_r}, \quad c_2 = \frac{1 - \frac{M}{4} + \frac{M}{4} \log\left(\frac{M}{4}\right)}{\left(1 - \frac{M}{4}\right)^2} e^{-t_r}, \tag{G2}$$

and t_r is given by (5.20). Then, we may use (5.13) to deduce that

$$x(s, t^*) = \int_0^s \frac{1}{h(s', t^*)} ds' = \frac{1}{\sqrt{c_1 c_2 t^*}} \arctan\left(\frac{s}{\sqrt{\frac{c_1}{c_2} t^*}}\right). \tag{G3}$$

REFERENCES

- ATASI, O., LEGENDRE, D., HAUT, B., ZENIT, R. & SCHEID, B. 2020 Lifetime of surface bubbles in surfactant solutions. *Langmuir* **36** (27), 7749–7764.
- BARTLETT, C., ORATIS, A.T., SANTIN, M. & BIRD, J.C. 2023 Universal non-monotonic drainage in large bare viscous bubbles. *Nat. Commun.* **14** (1), 877.
- BILLINGSLEY, P. 2017 *Probability and Measure*. John Wiley & Sons.

- BOUROUBA, L. 2021 The fluid dynamics of disease transmission. *Annu. Rev. Fluid Mech.* **53**, 473–508.
- BOWEN, M. & TILLEY, B.S. 2013 On self-similar thermal rupture of thin liquid sheets. *Phys. Fluids* **25** (10), 102105.
- BREWARD, C.J.W. 1999 The mathematics of foam. PhD thesis, Oxford University.
- BREWARD, C.J.W. & HOWELL, P.D. 2002 The drainage of a foam lamella. *J. Fluid Mech.* **458**, 379–406.
- BUCKMASTER, J.D., NACHMAN, A. & TING, L. 1975 The buckling and stretching of a viscida. *J. Fluid Mech.* **69** (1), 1–20.
- CHAMPOUGNY, L., ROCHÉ, M., DRENCKHAN, W. & RIO, E. 2016 Life and death of not so ‘bare’ bubbles. *Soft Matt.* **12** (24), 5276–5284.
- CHAMPOUGNY, L., SCHEID, B., RESTAGNO, F., VERMANT, J. & RIO, E. 2015 Surfactant-induced rigidity of interfaces: a unified approach to free and dip-coated films. *Soft Matt.* **11** (14), 2758–2770.
- CHOMAZ, J.-M. 2001 The dynamics of a viscous soap film with soluble surfactant. *J. Fluid Mech.* **442**, 387–409.
- CRASTER, R.V. & MATAR, O.K. 2009 Dynamics and stability of thin liquid films. *Rev. Mod. Phys.* **81** (3), 1131.
- DE WIT, A., GALLEZ, D. & CHRISTOV, C.I. 1994 Nonlinear evolution equations for thin liquid films with insoluble surfactants. *Phys. Fluids* **6** (10), 3256–3266.
- DEBRÉGEAS, G., DE GENNES, P.-G. & BROCHARD-WYART, F. 1998 The life and death of ‘bare’ viscous bubbles. *Science* **279** (5357), 1704–1707.
- DEIKE, L. 2022 Mass transfer at the ocean–atmosphere interface: the role of wave breaking, droplets, and bubbles. *Annu. Rev. Fluid Mech.* **54**, 191–224.
- DUBITSKY, L., STOKES, M.D., DEANE, G.B. & BIRD, J.C. 2023 Effects of salinity beyond coalescence on submicron aerosol distributions. *J. Geophys. Res.* **128** (10), e2022JD038222.
- EGGERS, J. 2014 Post-breakup solutions of Navier–Stokes and Stokes threads. *Phys. Fluids* **26** (7), 072104.
- EGGERS, J. & FONTELOS, M.A. 2015 *Singularities: Formation, Structure, and Propagation*. Cambridge University Press.
- ERININ, M.A., LIU, C., LIU, X., MOSTERT, W., DEIKE, L. & DUNCAN, J.H. 2023 The effects of surfactants on plunging breakers. *J. Fluid Mech.* **972**, R5.
- ERNEUX, T. & DAVIS, S.H. 1993 Nonlinear rupture of free films. *Phys. Fluids A: Fluid Dyn.* **5** (5), 1117–1122.
- FARSOIYA, P.K., POPINET, S., STONE, H.A. & DEIKE, L. 2024 A coupled Volume of Fluid–Phase Field method for direct numerical simulation of insoluble surfactant-laden interfacial flows and application to rising bubbles. <https://hal.science/hal-04461912>.
- GONNERMANN, H.M. & MANGA, M. 2007 The fluid mechanics inside a volcano. *Annu. Rev. Fluid Mech.* **39**, 321–356.
- GROS, A., BUSSONNIÈRE, A., NATH, S. & CANTAT, I. 2021 Marginal regeneration in a horizontal film: instability growth law in the nonlinear regime. *Phys. Rev. Fluids* **6** (2), 024004.
- HINCH, E.J. 1991 *Perturbation Methods*. Cambridge University Press.
- HOWELL, P.D. 1996 Models for thin viscous sheets. *Eur. J. Appl. Maths* **7** (4), 321–343.
- HOWELL, P.D. 1999 The draining of a two-dimensional bubble. *J. Engng Maths* **35**, 251–272.
- JIANG, X., ROTILY, L., VILLERMAUX, E. & WANG, X. 2022 Submicron drops from flapping bursting bubbles. *Proc. Natl Acad. Sci.* **119** (1), e2112924119.
- KITAVTSEV, G., FONTELOS, M.A. & EGGERS, J. 2018 Thermal rupture of a free liquid sheet. *J. Fluid Mech.* **840**, 555–578.
- LHUISSIER, H. & VILLERMAUX, E. 2009 Destabilization of flapping sheets: the surprising analogue of soap films. *C. R. Méc.* **337** (6–7), 469–480.
- LHUISSIER, H. & VILLERMAUX, E. 2012 Bursting bubble aerosols. *J. Fluid Mech.* **696**, 5–44.
- LIU, X. & DUNCAN, J.H. 2003 The effects of surfactants on spilling breaking waves. *Nature* **421** (6922), 520–523.
- MANIKANTAN, H. & SQUIRES, T.M. 2020 Surfactant dynamics: hidden variables controlling fluid flows. *J. Fluid Mech.* **892**, P1.
- MIGUET, J., PASQUET, M., ROUYER, F., FANG, Y. & RIO, E. 2020 Stability of big surface bubbles: impact of evaporation and bubble size. *Soft Matt.* **16** (4), 1082–1090.
- MIGUET, J., PASQUET, M., ROUYER, F., FANG, Y. & RIO, E. 2021 Marginal regeneration-induced drainage of surface bubbles. *Phys. Rev. Fluids* **6** (10), L101601.
- MYSELS, K.J., SHINODA, K. & FRANKEL, S. 1959 *Soap Films: Studies of Their Thinning and a Bibliography*. Pergamon Press.
- NÉEL, B. & VILLERMAUX, E. 2018 The spontaneous puncture of thick liquid films. *J. Fluid Mech.* **838**, 192–221.

Asymmetric Marangoni flow

- NGUYEN, C.T., GONNERMANN, H.M., CHEN, Y., HUBER, C., MAIORANO, A.A., GOULDSTONE, A. & DUFEK, J. 2013 Film drainage and the lifetime of bubbles. *Geochem. Geophys. Geosyst.* **14** (9), 3616–3631.
- ORON, A., DAVIS, S.H. & BANKOFF, S.G. 1997 Long-scale evolution of thin liquid films. *Rev. Mod. Phys.* **69** (3), 931.
- POPINET, S. & COLLABORATORS 2013–2024 Basilisk. <http://basilisk.fr>.
- POULAIN, S., VILLERMAUX, E. & BOUROUIBA, L. 2018 Ageing and burst of surface bubbles. *J. Fluid Mech.* **851**, 636–671.
- PROSSER, A.J. & FRANCES, E.I. 2001 Adsorption and surface tension of ionic surfactants at the air–water interface: review and evaluation of equilibrium models. *Colloids Surf. A* **178** (1–3), 1–40.
- RIBE, N.M. 2002 A general theory for the dynamics of thin viscous sheets. *J. Fluid Mech.* **457**, 255–283.
- RIBE, N.M. 2003 Periodic folding of viscous sheets. *Phys. Rev. E* **68** (3), 036305.
- SHI, X., FULLER, G.G. & SHAQFEH, E.S.G. 2022 Instability and symmetry breaking of surfactant films over an air bubble. *J. Fluid Mech.* **953**, A26.
- STONE, H.A. 1990 A simple derivation of the time-dependent convective–diffusion equation for surfactant transport along a deforming interface. *Phys. Fluids A: Fluid Dyn.* **2** (1), 111–112.
- TEICHMAN, J. & MAHADEVAN, L. 2003 The viscous catenary. *J. Fluid Mech.* **478**, 71–80.
- TIMMERMANS, M.-L.E. & LISTER, J.R. 2002 The effect of surfactant on the stability of a liquid thread. *J. Fluid Mech.* **459**, 289–306.
- VAYNBLAT, D., LISTER, J.R. & WITELSKI, T.P. 2001 Rupture of thin viscous films by van der Waals forces: evolution and self-similarity. *Phys. Fluids* **13** (5), 1130–1140.
- VERON, F. 2015 Ocean spray. *Annu. Rev. Fluid Mech.* **47**, 507–538.
- WEE, H., WAGONER, B.W. & BASARAN, O.A. 2022 Spontaneous rupture of surfactant-covered thin liquid sheets. *Phys. Rev. Fluids* **7** (9), 094005.
- ZAWALA, J., MIGUET, J., RASTOGI, P., ATASI, O., BORKOWSKI, M., SCHEID, B. & FULLER, G.G. 2023 Coalescence of surface bubbles: the crucial role of motion-induced dynamic adsorption layer. *Adv. Colloid Interface Sci.* **317**, 102916.